Composites Part C: Open Access 15 (2024) 100529

Contents lists available at ScienceDirect

Composites Part C: Open Access

journal homepage: www.sciencedirect.com/journal/composites-part-c-open-access

Genetic programming-based algorithms application in modeling the compressive strength of steel fiber-reinforced concrete exposed to elevated temperatures

Mohsin Ali [a], Li Chen [a,*], Qadir Bux Alias Imran Latif Qureshi [b,*], Deema Mohammed Alsekait [c,*], Adil Khan [d], Kiran Arif [e], Muhammad Luqman [f], Diaa Salama Abd Elminaam [g,h], Amir Hamza [f], Majid Khan [i]

[a] School of Civil Engineering, Southeast University Nanjing, China
[b] Department of Civil and Environmental Engineering, College of Engineering and Architecture, University of Nizwa, Birkat-al-Mouz, 616, Nizwa, Oman
[c] Department of Computer Science and Information Technology, Applied College, Princess Nourah Bint Abdulrahman University, P.O. Box 84428, Riyadh 11671, Saudi Arabia
[d] Department of Advanced Civil and Structural Engineering, University of Bradford, Bradford, West Yorkshire, BD7 1DP, UK
[e] Western Caspian University, Baku, Azerbaijan
[f] Department of Civil Engineering, University of Engineering and Technology, Peshawar, Pakistan
[g] MEU Research Unit, Middle East University, Amman 11831, Jordan
[h] Jadara Research Center, Jadara University, Irbid, 21110, Jordan
[i] Department of Civil Engineering, Southern Illinois University Edwardsville, Edwardsville, IL, 62026, USA

ARTICLE INFO

Keywords:
SFRC
Elevated temperature
Machine learning
Compressive strength
Predictive model

ABSTRACT

Steel-fiber-reinforced concrete (SFRC) has replaced traditional concrete in the construction sector, improving fracture resistance and post-cracking performance. However, extreme temperatures degrade concrete's material characteristics including stiffness and strength. The construction industry increasingly embraces machine learning (ML) to estimate concrete properties and optimize cost and time accurately. This study employs independent ML methods, gene expression programming (GEP), multi-expression programming (MEP), XGBoost, and Bayesian estimation model (BES) to predict SFRC compressive strength (CS) at high temperatures. 307 experimental data points from published studies were utilized to develop the models. The models were trained using 70 % of the dataset, with 15 % for validation and 15 % for testing. Iterative hyperparameter adjustment and trial-and-error refining achieved optimum predictions. All the models were evaluated using correlation (R) values for training, validation, and testing datasets. MEP showed slightly lower R-values of 0.923, 0.904, and 0.949 than GEP, which performed consistently with 0.963, 0.967, and 0.961. XGBoost had the greatest training R-value of 0.997 but dropped in validation (0.918) and testing (0.896). BES model exhibited commendable performance with scores of 0.986, 0.944, and 0.897. GEP and XGBoost exhibited great accuracy, with GEP sustaining constant accuracy across all datasets, highlighting its potency in predicting CS. Interpreting model predictions using SHapley Additive exPlanation (SHAP) highlighted temperature over heating rate. CS improved significantly as the steel fiber volume fraction (Vf) reached 1.5 %, plateauing thereafter. The proposed models are valid and accurate, providing designers and builders with a practical and adaptable method for estimating strength in SFRC structural applications, particularly under high-temperature conditions.

Abbreviation's list: ANN, Artificial neural network; CS, Compressive strength; DT, Decision tree; ETs, Expression trees; GEP, Gene expression programming; GP, Genetic programming; LIME, Local interpretable model-agnostic explanations; MLR, Multi-variable linear Regression; ML, Machine learning; MAE, Mean absolute error; MEP, Multi expression programming; OF, Objective function; ρ, Performance index; R, Correlation coefficient; RF, Random forest; RMSE, Root mean square error; RRMSE, Relative root means square error; SHAP, SHapley Additive exPlanations.

* Corresponding authors.
E-mail addresses: li.chen@seu.edu.cn (L. Chen), qadir.omran@unizwa.edu.om (Q.B.A.I.L. Qureshi), dmalsekait@pnu.edu.sa (D.M. Alsekait).

https://doi.org/10.1016/j.jcomc.2024.100529

Available online 15 October 2024

1. Introduction

Concrete is a fundamental and extensively employed construction material, playing a pivotal role in shaping the performance of buildings and infrastructure. However, concrete structures frequently face exposure to diverse and challenging environmental conditions, adversely influencing their structural stability [1]. These buildings are prone to fire hazards due to their reliance on electrical and gas appliances. For instance, high temperature adversely affects conventional concrete's performance due to its ingredients. Because of frequent fire-related disasters, it has been observed that fire poses significant hazards to the durability and stability of structures. Fire hazards are regarded as a potential threat to the safety of people and structures. Thus, the characteristics of concrete under high temperatures have captured the interest of researchers [2].

High temperature adversely affects the performance of conventional concrete due to its ingredients. Similarly, conventional concrete has shallow strain capacity and tensile strength. Therefore, various fibers can be used to enhance its load-carrying capacity. These fibers include steel [3], carbon [4], glass, polypropylene [5], synthetic fibers [6], recycled plastic [7], and basalt [8]. Incorporating short, discontinuous, and randomly dispersed fibers into conventional concrete [9–11] has emerged as a practical approach to improve the performance of concrete structures by mitigating shrinkage cracks and preventing micro-cracks during the transportation or installation of concrete members. Fiber-reinforced concrete is characterized by the integration of fibers into a cementitious matrix, forming a robust composite material. Previous research has established that integrating steel fibers (SF) into concrete results in enhancements to its strength properties [12–19]. Steel fiber-reinforced concrete (SFRC) exhibited remarkably improved strength compared to conventional concrete [20]. However, the complexity involved in determining the mechanical properties, particularly the widespread adoption of steel-fiber-reinforced concrete (SFRC) in structural engineering, is constrained primarily by challenges related to its compressive strength (CS). Therefore, various experimental investigations were conducted to assess the compressive strength (CS) of SFRC. Ahmad et al. [21] experimentally examined whether the surface temperature of concrete, when elevated to 100 °C, could increase heat transmission within the concrete. The primary factors affecting concrete failure in a fire are the heating rate, temperature, and the quality of structural components. Concrete's structural integrity and dependability hang predominantly on its compressive strength (CS). Consequently, numerous experimental inquiries have been conducted to examine the influence of temperature on CS. According to Technical Note 1681 by the National Institute of Standards and Technology (NIST), raising the temperature has an adverse impact on the CS of concrete [22]. Previous investigations have highlighted that the accumulation of pore vapor pressure within concrete and thermal stresses are the key factors contributing to explosive spalling and the degradation of strength. These factors substantially reduce the concrete strength when it is exposed to fire [23–27]. Therefore, fibers are added to concrete to mitigate the negative impacts of elevated temperature on concrete strength.

Steel fibers are predominantly employed as composite materials among various fiber types because of their thermal stability at elevated temperatures compared to other fibers [28]. SF in concrete can mitigate the impact of high temperatures during a fire by limiting the establishment of pore water pressure in the concrete. Additionally, SF helps bridge cracks within the concrete, facilitating better heat distribution and preventing concrete spalling [29–31]. In a post-fire scenario, including steel fibers significantly enhances the residual mechanical properties of concrete [32]. Residual compressive strength (CS) is important not only for structural fire protection design but also for structural repair. A study indicates a marginal increase in the residual CS of steel fiber-reinforced concrete (SFRC) between room temperature and 400 °C, attributed to accelerated cement hydration. However, a notable decline in residual CS occurs between 400 °C and 800 °C, with complete compromise beyond 800 °C [33]. The introduction of 1 % steel fibers by volume demonstrates the potential to enhance the residual CS of SFRC in the temperature range of 105–1200 °C [34]. However, it's reported that the rate of residual CS reduction in SFRC surpasses that of traditional concrete, possibly due to the distinct expansion properties of the concrete matrix and steel fibers [35]. The CS of SFRC is critical and a direct indicator of the overall mechanical performance. According to Lau and Anson [34], high-performance steel fiber reinforced concrete with 1 % steel fiber content, does not degrade at 1200 °C. Steel fiber enhances concrete's mechanical and thermal resistance. High temperatures damaged High-Performance Concrete (HPC) and Normal Strength Concrete (NSC), although HPC shows higher residual compressive, flexural, and modulus of elasticity. At 600 °C, HPC mixes lost more compressive strength than NSC at 400 °C. At high temperatures, HPC with more significant saturation percentages loses strength and has larger pores in the concrete body. Steel fibers slightly raise Poisson's ratio over the same mix without fibers. Poisson's ratio becomes zero at 1000 °C as exposure temperature increases. He also linked heated concrete's final color to its greatest temperature. In forensic fire temperature assessments for aggregate types, permanent charred colors may aid. Concrete changes color as temperature increases; knowing which colors correspond to which temperatures helps calculate fire temperature. Thus, color may indicate a concrete element's mechanical strength and maximum temperature following a fire. Studying the heating rate effect on concrete. Li et al. [36] found that at temperatures ranging from 500 to 800 °C, concrete's linear expanding rate (LER) consistently rises with rising temperature. Conversely, the heating rate influences the thermal expansion coefficient (TEC), resulting in higher LER and TEC values. ' The magnitude of the heating rate had a more significant influence on concrete distortion at high temperatures (500–800 °C) compared to lower temperatures (100–400 °C). Extended exposure to high temperatures (continuous temperature time) significantly influenced the deformation of the concrete, with more prolonged exposure resulting in higher LER and TEC values.

Numerous experiments have been conducted to evaluate how elevated temperatures impact the performance (especially CS) of SFRC. These studies have revealed that the performance of SFRC deteriorates due to chemical and physical alterations during the heating process [35]. Therefore, it is imperative to investigate the mechanical behavior of SFRC at elevated temperatures to provide valuable support for the endeavors of design and civil engineering professionals. However, collecting data and conducting experimental studies on FRC structures pose challenges because of the time-intensive nature of setting up and implementing tests and the extra expenses associated with labor and materials. Furthermore, evaluating concrete properties under elevated temperatures was discouraged due to the potential fire-related risks for operators and nearby structures.

Similarly, the limitations of numerical modeling stem from the model's formulation, computational processes, the nonlinear and stochastic nature of concrete, and the interpretation of results. Moreover, performing both experimental studies and numerical simulations on the strength of concrete at elevated temperatures demands significant time and resources. Therefore, a viable solution lies in adopting data-driven methodologies, such as machine learning (ML), to scrutinize the influence of elevated temperatures on the strength of SFRC.

In recent decades, the development of computing algorithms has accelerated the emergence of ML as a valuable approach for modeling and estimating concrete behavior. ML has earned acknowledgment as an effective method in numerous research fields, including composite structures [37] and concrete structures [38], due to its accurate estimations for desired mechanical properties [39,40]. ML algorithms can identify concealed patterns within large, intricate datasets [41]. ML algorithms can establish correlations between design input parameters, allowing for the prediction of target values based on previously conducted experimental tests. This enables intelligent product design by leveraging training approaches to make accurate predictions. Several

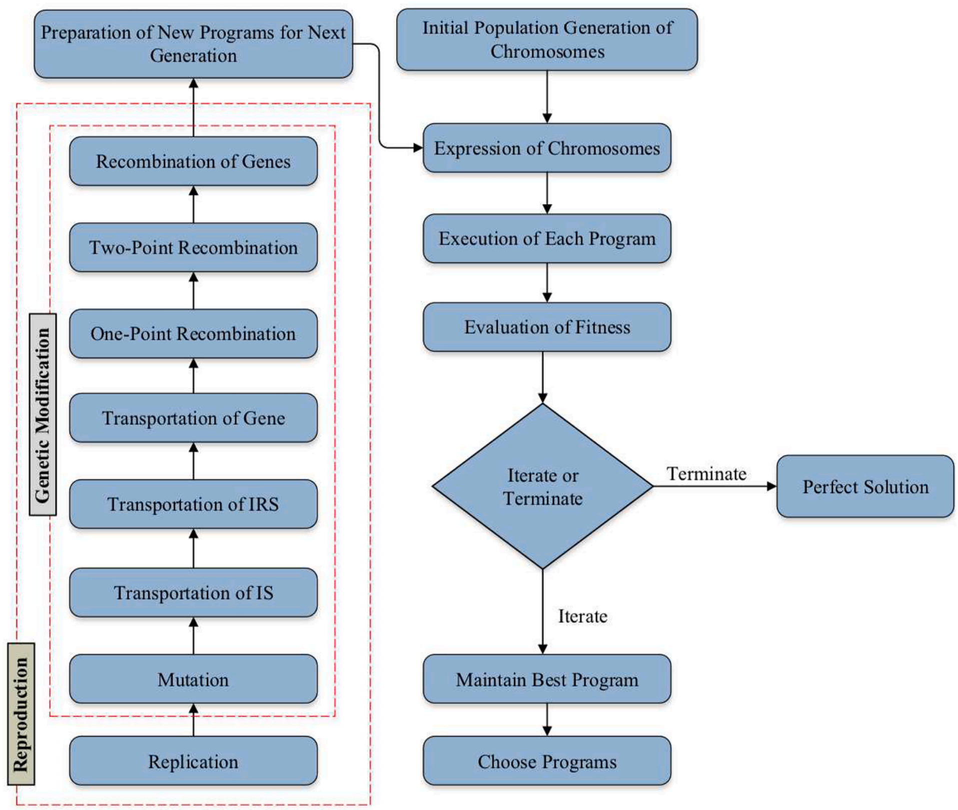

Fig. 1. GEP algorithm flowchart.

research studies have employed ML methods to forecast various mechanical characteristics of cement-based materials [42–44]. The Standard American (ACI 216) and European Codes (EN 1994-1-2) have overestimated the compressive strength of concrete subjected to fire with recycled PET Chips or steel fibers within 200 °C to 400 °C. For instance, Huang et al. [45] conducted an extensive investigation to predict the compressive strength (CS) of SFRCs by integrating the firefly algorithm with the support vector regression technique (SVM). Sun et al. [46] utilized a combination of the random forest (RF) method and the beetle antennae search (BAS) algorithm to assess the impact of incorporating waste steel slag in concrete on the CS. Ashrafuddin et al. [47] applied the metaheuristic-based multivariate adaptive regression splines (MARS) to capture insights on natural zeolitic concrete (NZC's) post-fire behavior and matched experimental data which reveals the climatic, environmental, and economic benefits of natural pozzolans. Memarzadeh et al. [48] employed GEP with 149 datasets to forecast the elastic modulus of recycled aggregate concrete-filled steel tubes at comparatively higher temperatures under axial load. Almustafa and Nehdi [49] applied an innovative generative adversarial network approach to forecasting the structural behavior of SFRC beams under blast loading conditions originating from a remote source. Concerning the influence of temperature on predicting the strength properties of SFRC. Chen et al. [50] employed the convolutional neural network technique to estimate the CS of fiber-reinforced concrete. After exposure to 600 °C, the specimens showed a higher compressive strength reduction rate than other temperatures, with some specimens having the lowest and highest strength reduction of 60.9 % and 82 %, respectively, relative to room temperature. For the temperatures after 600 °C, certain specimens exhibited the lowest and highest strength drop rates of 60.9 % and 82 %, respectively, compared to room temperature [44]. Namatzadeh and Shahmansouri [44] obtained the optimal value of design parameters using the response surface method with the development of a closed-form equation to forecast compressive strength via the GEP method. These studies highlighted the potential of various ML techniques in accurately estimating the properties of SFRC materials under different scenarios and temperatures.

However, limited research studies on ML are available to assess the compressive strength (CS) of SFRC at elevated temperatures. Chen et al. [50] used a conventional neural network to analyze the influence of elevated temperatures on the compressive strength (CS) of SFRC. The reduction in compressive strength (CS) of SFRC is impacted by both the heating rate and elevated temperature [51]. Literature reviews have revealed a lack of research on evaluating the compressive strength (CS) of SFRC under elevated temperatures. Torkan et al. [52] utilized various ML algorithms to predict the CS of SFRC under elevated temperature conditions, determining that a stacked ML method yielded the highest accuracy, achieving an R^2 value of 0.92 [52]. Likewise, another researcher [53] employed ML algorithms, utilizing ANFIS and ANN, to predict the CS of SFRC under elevated temperatures. However, none of the previously published studies formulated an empirical equation based on machine learning algorithms. To address this research gap, the current study aims to formulate an empirical equation for the compressive strength (CS) of SFRC utilizing ML algorithms like GEP and MEP. The primary objectives of this research include (a) the formulation of a highly accurate and reliable predictive model for CS of SFRC that takes into account both heating rate and elevated temperature, (b) formulating an empirical expression for the CS of SFRC using ML, and (c) performing SHAP analysis from both local and global perspective to explore the impact of various input factors on the compressive strength (CS) of SFRC.

2. Background of employed ML methods

2.1. Gene expression programming (GEP)

Koza [54] introduced genetic programming (GP) as a method based

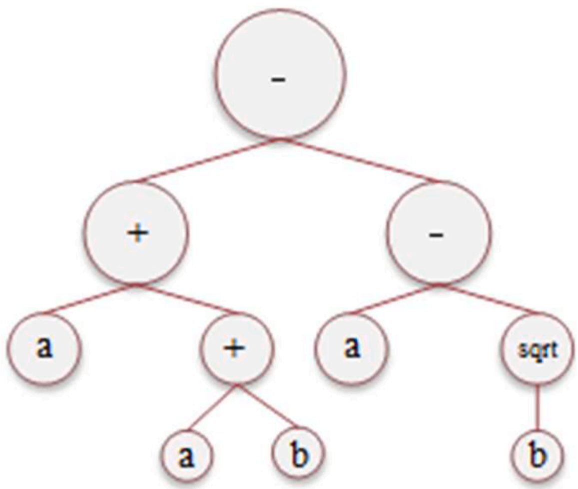

Fig. 2. Expression tree of chromosome.

on Darwin's theory of natural selection. GP is derived from genetic algorithms (GA) and employs similar operators with minor distinctions. GP and GA utilize crossover and mutation as standard operators [55]. However, the critical distinction is that GP produces a mathematical program on a given set of records, whereas GA focuses on solving a mathematical model. Ferreira [55] made advancements to GP by introducing gene expression programming (GEP), which produces an expression tree (ET) or mathematical expression based on given inputs. GEP comprises five components: terminal condition, function set, control parameters, terminal set, and fitness function. These elements combine to create ETs or mathematical programs of various shapes and sizes [56].

The main distinction between GEP and GP is in the representation of the mathematical model. GEP utilizes strings characters of fixed length, while GP employs character strings with variable length. GEP offers several advantages, one of which is the ease of generating genetic diversity at the chromosome level, attributed to the inherent genetic mechanisms of this approach. Furthermore, GEP is regarded as a multigenic method, enabling the evolution of more intricate and nonlinear programs that encompass multiple subprograms [56]. Fig. 1 illustrates the GEP method's process, which commences by randomly designing chromosomes with a consistent length for each evolving equation or individual. The expression tree of a chromosome is depicted in Fig. 2. Subsequently, the chromosomes undergo expression, and the accuracy of each individual is assessed. Based on their precision, the equations are identified, and a reproduction process is carried out. This iteration continues until the most suitable expression is obtained. Different operations, including mutation and crossover, are utilized to modify the population and support the evolution of equations as shown in Fig. 3 [56].

2.2. Multi-expression programming (MEP)

Oltean and Dumitrescu [57] proposed a unique variant of genetic

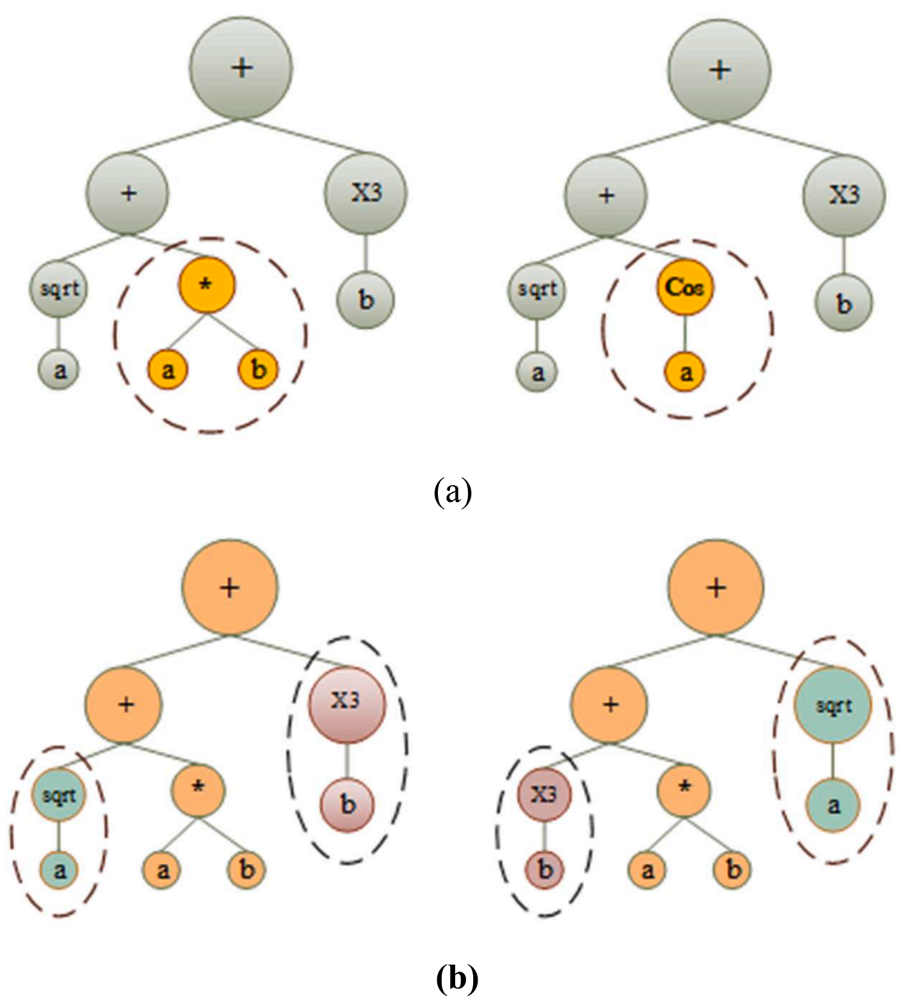

Fig. 3. GEP (ETs) employ LISP language for both (a) mutation and (b) crossover.

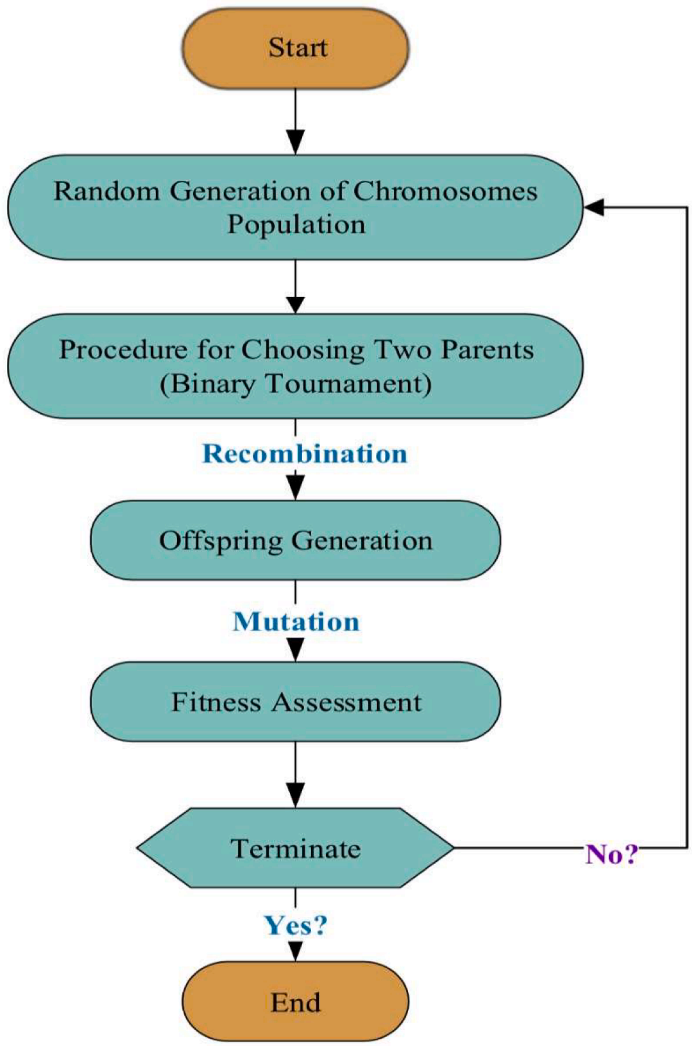

Fig. 4. MEP algorithm flowchart.

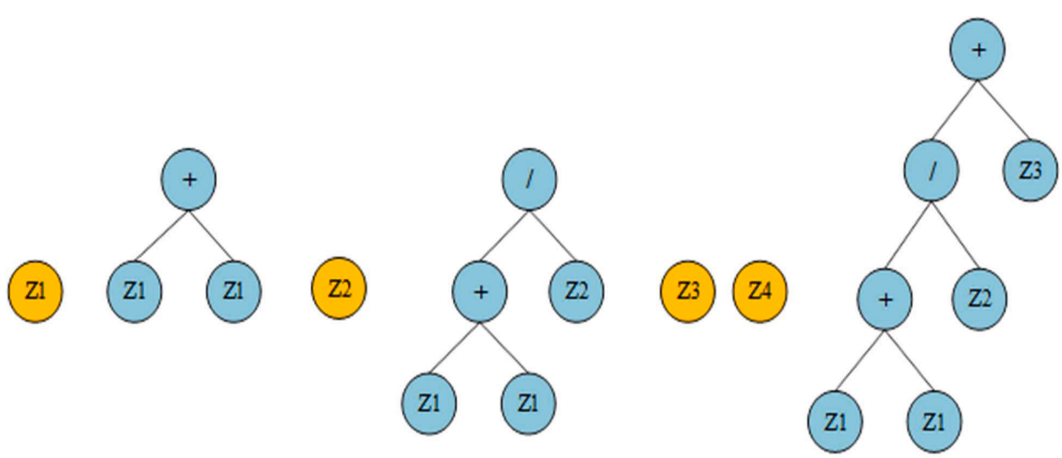

Fig. 5. Architecture of the MEP algorithm.

programming known as multi-expression programming (MEP). MEP utilizes linear chromosomes to develop mathematical programs and has the capability to encode multiple equations within an individual chromosome. In contrast to other branches of GP, The MEP approach diverges from traditional genetic programming by not storing a single mathematical program per chromosome. Instead, fitness values assigned to individuals are leveraged to identify the most suitable encoded solution. To achieve the optimal mathematical expression for the dependent attribute using the given inputs, the MEP initiates by producing an initial population of individuals without any predefined function.

Table 1
Database statistical summary.

Statistics	Input variables					Output
	T (°C)	HR (°C/mm)	L(mm)	V_f (%)	D (μm)	CS (MPa)
Median	450	3.33	25	1	220	46.8
Mean	451.83	5.06	26.62	1.05	400.58	68.92
Mode	20	5	13	0	200	20
Standard Deviation	336.67	6.55	17.20	0.91	287.19	59.17
Range	1180	30	54	5	1470	218.5
Kurtosis	-1.09	8.32	0.62	0.54	1.88	-0.36
Sample Variance	113,348.4	42.86	295.86	0.82	82,476.07	3501.07
Skewness	0.17	2.84	0.80	0.89	1.31	0.91
Maximum	1200	30	60	5	1500	220
Minimum	20	0	6	0	30	1.5

Subsequently, The MEP algorithm employs a binary tournament process to select two parents from the population. These chosen parents undergo recombination using an unaltered crossover probability, producing two offspring. The offspring then experience mutation. In the current population, the worst-performing individual is replaced with the best offspring obtained. Fig. 4 illustrates the MEP technique, showcasing these steps. Additionally, the architecture of the MEP algorithm is depicted in Fig. 5.

2.3. XGBoost

XGBoost, which stands for eXtreme Gradient Boosting [58], is a type of Gradient Boosting Machine (GBM) used mainly for regression and classification in predictive modeling. GBM models have consistently demonstrated better performance compared to many other machine learning algorithms on various datasets [59]. XGBoost works as an ensemble method, where each new model is created to correct the mistakes of the previous ones, and they are combined to generate the final prediction. It is generally faster than other ensemble classifiers, such as AdaBoost. XGBoost's effectiveness has made it widely used and popular in data science challenges, especially among Kaggle competitors and industry professionals [60]. Moreover, XGBoost is a parallelizable algorithm, meaning it can take advantage of multi-core processors. This capability enables it to handle and train on very large datasets efficiently.

2.4. Bayesian estimation model

Bayesian machine learning is a specialized area of machine learning that integrates Bayesian inference principles with computational models to enhance predictions and decision-making [61]. Rooted in the Bayesian framework, this approach models uncertainty by updating prior beliefs based on new data. Unlike conventional machine learning techniques that often provide point estimates, Bayesian machine learning uses probability distributions over model parameters and predictions, offering a more detailed understanding of uncertainty [62]. It is applicable across various areas such as classification, regression, clustering, and reinforcement learning [63]. Bayesian methods excel in managing uncertainty, allowing flexible modeling, and incorporating prior knowledge, but they face challenges like computational complexity and scalability. Future advancements in Bayesian machine learning aim to develop more scalable algorithms, enhance computational efficiency, integrate Bayesian methods with deep learning, and improve interpretability.

3. Methodology

3.1. Data collection

A comprehensive dataset was gathered from published experimental studies, including various input parameters affecting SFRC performance. The dataset consisted of 307 experimental analyses of SFRC extracted from 44 studies. These experimental tests involved the measurements of heating rate and temperature in SFRC [24,33,64–99]. The input variables include fiber diameter (D), fiber length (L), volume fraction (V_f), heating rate (HR), and temperature (T). The response parameter is the CS of SFRC. The primary objective of this study is to develop machine learning-based models capable of accurately predicting the compressive strength (CS) of SFRC under high-temperature conditions. The datasets utilized in this research comprise abundant data on SFRC, typically with hooked ends, exposed to high-temperature conditions. By thoroughly examining published studies, it was identified that various additional variables influence the performance of SFRC. However, for the specific focus of this study on the impact of high temperatures on predicting the CS of SFRC, test data that did not consider heating rate and temperature factors were excluded from the dataset.

Preprocessing of the data was done with a nominal filter. The imputation method was used for missing values. Though overall, no missing values were found, the data was processed via a series of cleaners. The replacement of numbers was given the preference of order by closest percentile subgroup 84th percentile, median, and mean. Both Regression and multiple imputations were used as cleaning agents. The outlier detection followed both ML techniques, such as anomaly detection algorithms and statistical methods, including IQR and Z-score techniques. The Z-score normalization was preferred over the min-max method, which had limited variability to cover the standardized data for improved accuracy of ML models. It is to be mentioned that the convergence rate of almost all the applied models, mainly GEP, was superior to the same model when applied to rough data.

Table 1 gives a descriptive statistical analysis of the acquired dataset. The temperatures range from 20 °C to 1200 °C, while fiber dosage ranges from 0 to 5 %. In addition, the CS of SFRC ranges from 1.5 to 220 MPa. It is reported that the skewness and kurtosis of a reliable dataset must be in the ranges of ±3 and ±10, respectively [100]. The parameters in the acquired dataset have the skewness and kurtosis values in the recommended ranges. Before further analysis, examining the correlations between these numerical parameters is essential. Pearson's correlation coefficient (r), ranging from -1 to 1, is commonly employed to measure the linear correlation between two parameters [101]. It is crucial to address the issue of multi-collinearity, which arises when there are high correlations between predictor variables [102]. Fig. 5 depicts the r determined for all possible combinations of parameters. The analysis reveals no evidence of multi-collinearity, as all correlation coefficients, whether positive or negative, are below 0.80. To ensure unbiased model assessment, the datasets were randomly divided into validation, training, and testing sets, with 70 % allocated for training, 15 % for validation, and 15 % for testing purposes. In addition, the distribution of the selected explanatory variables and output property is provided in Fig. 7.

3.2. Model development

This research utilized two modeling algorithms, GEP, MEP, XGBoost, and Bayesian estimation method (BES) models to predict the CS of SFRC. The models were developed by initializing the algorithms, applying genetic operators, and iteratively refining the predictions until convergence.

3.2.1. GEP model

This study employed the GEP approach to formulate a mathematical expression for predicting the CS of SFRC. As stated in prior research

Table 2
GEP model hyperparameter settings.

Parameter	Setting
General	
Linking function	Multiplication
Genes	4
Chromosomes	250
Head size	10
Set of functions	*, /, +, -, Exp, Inv, Ln, 3Rt, x^2, x^3, x^4
Numerical constants	
Lower bound	-10
Upper bound	10
Data type	Floating-point
Constant per gene	10
Genetic operators	
Random cloning	0.00102
Permutation	0.00546
Inversion rate	0.00546
Mutation	0.00138
RIS transportation rate	0.00546
IS transportation rat	0.00546
Recombination rate	0.00277
Dc mutation	0.00206
Gene transportation rate	0.00277
RNC mutation	0.00206

Table 3
MEP model hyperparameter settings.

Parameter	Optimized value
No. of subpopulations	50
Tournament size	2
Subpopulation size	250
Code length	50
Crossover probability	0.9
Functions probability	0.5
Variables probability	0.5
Mutation probability	0.01
Functions	+, -, *, /, Power, Exp, Sqrt, Tan, Sin, Cos, ASin, ATan, ACos

Table 4
Hyperparameters tuning (skopt-BayesSearchCV) for XGBoost model.

Parameter	Space/Value
n_estimators	(50, 1000)
learning_rate	(0.001, 0.2, 'uniform')
max_depth	(3, 26)
min_child_weight	(1, 3)
Subsample	(0.5, 1.0, 'uniform')
colsample_bytree	(0.5, 1.0, 'uniform')

Table 5
Hyperparameters tuning (Bayesian Optimization).

Parameter	Space/Value
"objective"	reg: squared error
"max_depth"	int(max_depth)
"gamma"	gamma
"colsample_bytree"	colsample_bytree
"learning_rate"	0.01
"n_estimators"	1000
"min_child_weight"	1
"subsample"	0.2
"max_depth"	(3, 26)
"gamma"	(0,5)
"colsample_bytree"	(0.3,0.9)

[103,104], determining the optimal parameters for the GEP model implies a procedure of trial and error. Multiple trials were conducted in this study to identify the best hyperparameters for the GEP model tailored to the specific problem. The GEP algorithm was initiated by creating a random population with specific parameters, including linking functions, gene count, chromosome count, genetic operators, and head size. The dataset was initially loaded into the GeneXpro Tools 5.0 interface, designating attributes as predictors and targets. Subsequently, the dataset was split into 70 % for training, 15 % for validation, and 15 % for testing. The K-fold method was preferred over the Leave one out (LOO) method for cross-validation and data splitting with folds out of which 9 were for training and 3 for validation. This will ensure that variance is compensated, and overfitting issues are addressed. Table 2 illustrates the problem's initialization with assigned values to input parameters, such as a gene count of 4, a chromosome count of 200, and a head size of 10. Linking operators were assigned to different genes based on relevant information from the literature. The model reached its optimal state through iterative experimentation by achieving higher correlation coefficient (R) values and lower errors, such as mean absolute error (fitness function).

3.2.2. MEP model

Several MEP hyperparameters need to be specified before the modeling process to ensure the establishment of a robust and versatile model. These relevant parameters are selected based on suggestions from the literature and through a continuous iterative process. The population size inherently determines the number of programs to be generated. While utilizing a larger population size in the model may result in more precise outcomes, it could also extend the convergence time. This trade-off highlights the need to balance computational resources with the desired precision in the model's performance. The MEP process begins with the initialization of expressions and functions. Subsequently, the population of chromosomes is randomly expanded through connecting functions by binary selection. As the population of chromosomes reaches a certain threshold, offspring are generated and assessed using an assessment function. The MEP evolution proceeds through a series of steps: initiating with a random population of chromosomes, selecting two parents through a binary tournament, executing recombination with a predetermined crossover frequency, producing two offspring by combining the selected parents, mutating the offspring, and replacing the least fit individuals in the population with the newly generated ones. This iterative process continues until convergence is achieved. The cyclical nature of these steps ensures the refinement of the MEP algorithm until it reaches a state of convergence, optimizing its performance in predicting the compressive strength of SFRC. Table 3 summarizes the variables employed in the study, with all the values calculated through multiple trials using various combinations. The MEP technique was implemented in MEPX (Version. 2023.4.3.0)

3.2.3. XGBoost model

Table 4 displays the hyperparameters tuning for the Extreme Gradient Boosting (XGBoost) model.

3.2.4. Bayesian estimations model

In Table 5, the hyperparameters tuning for the Bayesian Estimations Model (BES) are provided.

3.3. Performance evaluation metrics

The effectiveness of the proposed GEP and MEP techniques in predicting the compressive strength of SFRC was evaluated using several standard statistical measures: RRMSE, MAE, RMSE, R, and RSE. Additionally, the performance index (ρ) was also calculated. These performance metrics are reparented in Eqs. (1)–(7) were utilized to assess the accuracy of the models [105].

$$\mathrm{RMSE}=\sqrt{\frac{\sum_{i=1}^{n}(\mathrm{ei}-\mathrm{mi})^{2}}{\mathrm{n}}} \tag{1}$$

Table 6
External validation metrics.

S.No	Expression	Conditions	Suggested by
1	$k = \frac{\sum_{i=1}^{n}(ei \times mi)}{ei^2}$	$0.85 < k < 1.15$	[108]
2	$k' = \frac{\sum_{i=1}^{n}(ei \times mi)}{mi^2}$	$0.85 < k' < 1.15$	
3	$R^2 = 1 - \frac{\sum_{i=1}^{n}(mi - e_i^{\circ})^2}{\sum_{i=1}^{n}(mi - m_i^{o})^2}$	$R^2 \cong 1$	[109]
	Where, $e_i^{\circ} = k \times m_i$		
	$R_{\circ}^2 = 1 - \frac{\sum_{i=1}^{n}(ei - m_i^{\circ})^2}{\sum_{i=1}^{n}(ei - e_i^{o})^2}$	$R_{\circ}^2 \cong 1$	
	Where, $m_i^{\circ} = k' \times e_i$		
	$R_m = R^2 \times (1 - \sqrt{\lvert R^2 - R_o^2 \rvert})$	$R_m > 0.5$	
4	$m = \frac{R^2 - R_{\circ}^2}{R^2}$	$m<0.1$	[110]

$$MAE = \frac{\sum_{i=1}^{n}|ei - mi|}{n} \tag{2}$$

$$RSE = \frac{\sum_{i=1}^{n}(mi - ei)^2}{\sum_{i=1}^{n}(\bar{e} - ei)^2} \tag{3}$$

$$R = \frac{\sum_{i=1}^{n}(ei - <ct> \bar{e} <ot> i)(mi - \overline{m}i)}{\sqrt{\sum_{i=1}^{n}(ei - <ct> \bar{e} <ot> i)^2 \sum_{i=1}^{n}(mi - \overline{m}i)^2}} \tag{4}$$

$$RRMSE = \frac{1}{|<ct> \bar{e} <ot>|} * \sqrt{\frac{\sum_{i=1}^{n}(ei - mi)^2}{n}} \tag{5}$$

$$\rho = \frac{RRMSE}{1 + R} \tag{6}$$

$$OBF = \left(\frac{n_T - n_v}{n}\right) * \rho_T + 2\left(\frac{n_v}{n}\right) * \rho_V \tag{7}$$

where "ei" represents the actual output value for the ith sample, "mi" indicates the predicted output value. The averages of all experimental and forecasted output values are denoted as "ēi" and "m¯i" respectively. The variable "n" stands for the total sample number, "V" represents the number of validations, and "T" denotes the training dataset.

The R-value is a standard measure to evaluate the correlation between the model's predicted values and the experimental outputs. A strong correlation is typically inferred when R exceeds 0.8. The lower RMSE and MAE values, closer to zero, signify minimal prediction error. In summary, a higher R-value and smaller values of RRMSE, RMSE, MAE, and RSE suggest a well-developed model. The "ρ" ranges from 0 to infinity, and a value approaching zero signifies optimal model accuracy [106].

Excessive training of data points can lead to overfitting in various machine learning methods, resulting in lower training errors but higher validation and testing errors. The objective function (OBF) is utilized to select the best estimation model that mitigates overfitting to overcome this issue. The OBF, expressed as Eq. (7), is minimized, aiming for a lower OBF value (close to 0), indicating a higher predictive model performance [107]. The OBF considers the influence of RRMSE, R, and the relative percentage of dataset records. This study examined various combinations of fitting attributes, and the model with the lowest OBF was selected as the optimal one. Furthermore, the validity of the developed machine learning models is appraised using evaluation criteria recommended in the literature, as outlined in Table 6.

3.3.1. SHapley Additive exPlanations (SHAP)

The SHAP method is a model-agnostic approach to explaining individual predictions generated by ML models [111]. SHAP analysis is a powerful method used in ML to explain and interpret model predictions. Developed from cooperative game theory, SHAP assigns a value to each attribute in a prediction, showing its contribution to the model's output. By clearly understanding how individual features influence predictions, SHAP helps users gain insights into model behavior and identify which factors are most influential. Unlike other interpretation methods, SHAP considers the interactions between features, offering a more comprehensive view of model decision-making. By assigning an importance value to each feature based on conditional expectations, SHAP values are derived. These values are then visualized to illustrate the contribution of each feature relative to a base value, typically representing the average of the examinations. Islam et al. [112] effectively explained the effect of crucial physical parameters like curing age, cement, and water on the strength of High-Performance Concrete (HPC), giving a reliable idea of explaining physical feature dependence on target from experimental data. Kashem et al. [113] examined the feasibility of using artificial intelligence (AI) and the SHAP algorithm to assess the workability of concrete in construction. The study focused on the significant impact of water content, coarse particles, and fine aggregates on the flow properties of concrete. Tipu et al. [114] propose a novel method combining reclaimed coarse sand with Newton's Boosted Back-propagation Neural Network (NB-BPNN) model to predict accurately concrete's compressive strength. The technique achieves an impressive R2 score of 0.95. Additionally, SHAP analysis highlighted the significant influence of crucial ingredients such as GGBS, Binding agent, Cement, Water/Binder proportions, and Superplasticizer. Many other researchers have evaluated many physical feature interpretations from SHAP, yielding valuable hints in practical decision-making.

Notably, while the SHAP approach considers all attributes and their order, it can be computationally intensive for larger models. However, its ability to uncover the inner workings of complex ML models makes SHAP a valuable tool for both model developers and end-users seeking to understand and trust the decisions made by ML/AI models.

4. Results and discussion

4.1. GEP formulation

To forecast the CS of SFRC, typical ETs were developed for the GEP algorithm, as depicted in Fig. 8. ETs of the GEP model present various components, including constants, functions, operators, and variables [115]. These ETs incorporated fundamental mathematical operators, such as addition, subtraction, multiplication, division, 3Rt, x^3, log, and x^2. Once the GEP model was developed, the ETs were decoded to obtain an easy and simplified mathematical expression representing the CS regarding the input parameters. By utilizing the hyper-parameter configurations specific to the GEP model, the transformation of ETs into simplified mathematical expressions is obtained using the Karva notation or K-expression [107], as given in Eq. (8. This simplified equation, derived from the GEP model, effectively estimates the CS of SFRC subjected to elevated temperatures.

$$CS = A \times B \times C \times D \tag{8}$$

where,

$$A = (13.38 \times (D + 664.07 \times L)) \tag{9}$$

$$B = (1.89 / L) \tag{10}$$

$$C = \left(\log\left(D - 13.83 + HR^4 \times VF^4\right)\right) \tag{11}$$

$$D = (1 / (18.74 + T + D + (T / L) - L)) \tag{12}$$

4.2. Developed models performance

This section thoroughly analyzes the developed ML models to

Table 7
Performance summary of the models.

Model	GEP			MEP		
	Training	Validation	Testing	Training	Validation	Testing
MAE	10.409	11.104	10.235	15.021	17.651	13.706
RRMSE	0.238	0.213	0.214	0.339	0.375	0.250
RMSE	16.141	15.999	14.521	22.983	28.136	16.929
RSE	0.073	0.065	0.079	0.148	0.202	0.107
P	0.121	0.108	0.109	0.176	0.197	0.128
R	0.963	0.967	0.961	0.923	0.904	0.949
OBF	0.1291			0.1306		
Model	XGBoost			BES		
	Training	Validation	Testing	Training	Validation	Testing
MAE	2.198	12.027	10.815	4.645	4.307	8.484
RRMSE	5.128	23.927	24.687	11.769	9.347	24.128
RMSE	3.479	17.975	16.728	8.135	7.022	16.349
RSE	0.003	0.082	0.104	0.018	0.013	0.100
P	2.568	12.477	13.024	5.927	4.807	12.722
R	0.997	0.918	0.896	0.986	0.944	0.897
OBF	0.114			0.0941		

Table 8
External validation of the models.

Conditions	**$0.85 < k < 1.15$**	**$0.85 < k' < 1.15$**	**$R^2 \cong 1$**	$R_o^2 \cong 1$	**$R_m > 0.5$**	**$m < 0.1$**
GEP	0.9711	0.9982	0.9734	0.9999	0.8149	0.0272
MEP	0.9313	1.0046	0.9327	0.9996	0.6914	0.0718
XGBoost	0.9695	1.0068	0.9311	0.9233	0.8647	0.0275
BES	0.9989	0.9853	0.9580	0.9549	0.9167	0.0034

validate their capability to forecast the CS of SFRC accurately under elevated temperatures. Therefore, regression slope analysis, error analysis, and statistical indicator evaluation were conducted.

4.2.1. Regression slope analysis

The regression line slopes are reliable indicators of the model's accuracy and predictive capabilities. Fig. 9 illustrates the regression plots comparing the estimated outcomes of the generated models (GEP and MEP) with the corresponding experimental records. Generally, a regression slope above 0.8 indicates a strong correlation between experimental and model output. The GEP model demonstrated a regression slope of 0.92 for training, 0.91 for validation, and 0.93 for testing, respectively. This significantly surpasses the 0.8 threshold, underscoring the robustness of the GEP model in estimating the CS of SFRC exposed to higher temperatures. Similarly, the MEP model exhibited a slope of 0.86 for training, 0.77 for validation, and 0.97 during the testing phase. XGBoost and BES models also performed well during training, demonstrating slopes of 0.98 and 0.96, respectively. However, a drop in their regression slopes was observed, with values of 0.893 and 0.890 for validation, and 0.86 and 0.89 for testing. Notably, the fitting lines of training, validation, and testing in the GEP model closely align with the ideal fitting line, while those of the MEP model deviate from the ideal fitting line.

4.2.2. Error analysis

The error assessment of the developed models is presented in Figs. 10 and 11. Notably, the GEP model predictions closely align with the experimental values in the training, validation, and testing stages, as shown in Fig. 10(a)**.** On the contrary, the MEP model deviates from the trend of experimental values, as shown in Fig. 10(b)**.** The error histograms of the developed models are provided in Fig. 11**.** The GEP model showed 86.06 % of the prediction records within the error range of ±20 MPa. Likewise, the MEP model exhibited 73.05 % prediction records within the error range of ±20 MPa. Additionally, for the XGBoost model, 93.15 % of the predictions, and for the BES model, 94.78 % of the predictions fall within the error range of ±20.

4.2.3. Statistical indicator evaluation

Several metrics were employed to evaluate the efficacy of the developed models comprehensively. The summarized statistical evaluation in Table 7 includes accuracy metrics (R) and error metrics like MAE, RMSE, RRMSE, RSE, OBF, and ρ. The GEP model exhibited higher R-values of 0.963 for training, 0.967 for validation, and 0.961 for testing, accompanied by MAE values of 10.409 for training, 11.104 for validation, and 10.235 for testing. Furthermore, the GEP model's performance index (ρ) for both sets remained below 0.20, underscoring the robust efficacy in predicting the output. Similarly, the MEP model showed R-values of 0.923 for training 0.904 for validation, and 0.949 for testing. The MAE values of the MEP model were 15.021 for training, 17.651 for validation, and 13.706 during testing. Moreover, both the XGBoost and the BES models performed well during training, achieving R-values of 0.997 and 0.986, respectively. However, while XGBoost saw a decline in validation (0.918) and testing (0.896), the BES model maintained relatively stable performance with values of 0.944 in validation and 0.897 in testing. GEP consistently demonstrated strong accuracy across all datasets, further emphasizing its reliable performance in predicting CS. The OBF values of both models are below 0.20, demonstrating that the issue of model overfitting is satisfied. Moreover, the overall statistical indicators are illustrated in Fig. 12**,** showing that the GEP model in training exhibits the highest value for R and the lowest values for other error indicators. The statistical analysis demonstrated a close agreement between the actual and model values for both the developed ML models. However, GEP outperformed all the other ML models, displaying the highest R and minimal errors, thus establishing itself as a reliable predictor of the CS of SFRC under elevated temperatures.

The developed ML models also satisfied external validation. The generated GEP model underwent various external statistical validation checks, as detailed in

Table 8, to evaluate their accuracy and reliability. One criterion used for external validation involved ensuring that the regression line slopes (k or k') closely approached one, as suggested in prior research [108,116,117]. Another criterion, the confirming indicator (Rm), introduced by Roy [115], was employed to gauge a model's predictability. This demonstrates that the requirement for Rm to exceed 0.5 has been fulfilled, as shown in Table 5. This establishes that the models meet the criteria for external validation, attesting to their realism and negating any notion of being a mere correlation between output and input variables. Consequently, the developed models, particularly the GEP model, have the potential to provide precise and accurate predictions for the compressive strength of SFRC exposed to elevated temperatures.

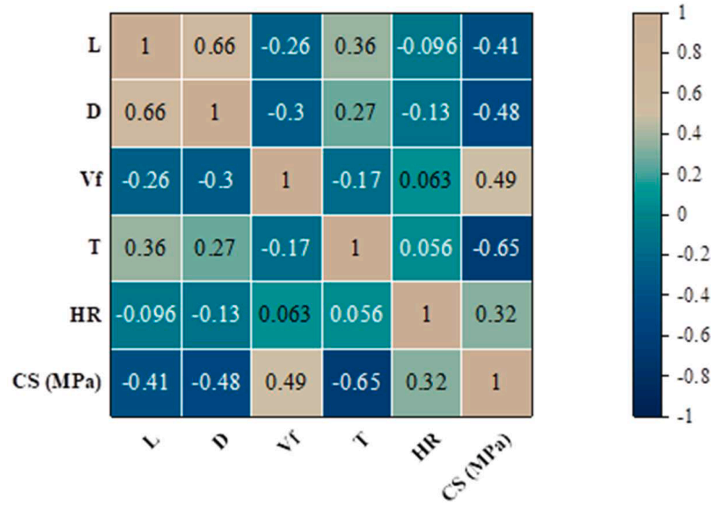

Fig. 6. Pearson correlation diagram.

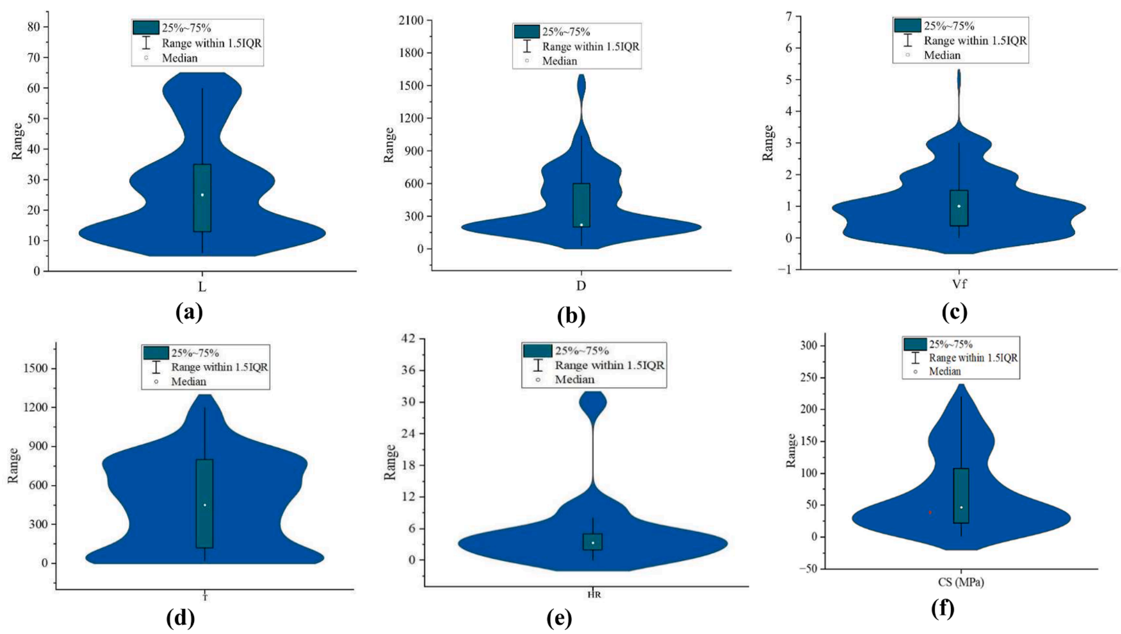

Fig. 7. Violin plots with box plots for variable distribution.

4.3. Comparison of the developed model

This section compares the efficacy and performance of the developed models. For instance, the GEP model outperformed the MEP model, showing a 10.5 % higher R-value in training, 5.5 % higher in validation, and 1.25 % higher in testing. Although the XGBoost model exhibited a 3.41 % higher R-value in training and a 78.88 % lower MAE value than the GEP model, its R-value dropped by 5.067 % in validation and 6.76 % in testing compared to GEP. The BES model followed a similar trend, demonstrating superior performance during the training phase with a 2.33 % higher R-value, but its performance declined in the validation and testing phases.

To conduct a more in-depth comparative analysis of the models' performance, Fig. 13 presents a Taylor diagram. Developed by Karl E. Taylor [118], this diagram serves as a visual tool for evaluating the accuracy of prediction models, illustrating which model is the most robust and closest to the original data. Multiple models are plotted in a single diagram, enabling a relative assessment of their accuracy concerning the benchmark (actual data) [118,119]. Additionally, the diagram offers a comprehensive way to compare multiple models in terms of their correlation, variance, and RMSE relative to the reference data. Notably, the GEP model closely aligns with the reference symbol in validation, training, and testing, indicating its exceptional predictive precision.

4.3.1. Developed models comparison with multiple linear regression (MLR)

MLR is a statistical method that estimates an outcome variable based on multiple explanatory factors [120]. This study employs the MLR technique on the experimental datasets to assess its performance compared to the developed ML models. The MLR model was utilized to examine the correlation between the inputs and the target variable, allowing for a comparative evaluation of its predictive capabilities alongside the developed ML models. The mathematical expression developed for the MLR technique in this study is given by Eq. (13

$$\begin{aligned} CSMLR = {} & 91.5842 + (0.2116 \times L) + (-0.0473 \times D) \\ & + (21.1519 \times V_f) + (-0.1011 \times T) + (2.819 \times HR) \end{aligned} \tag{13}$$

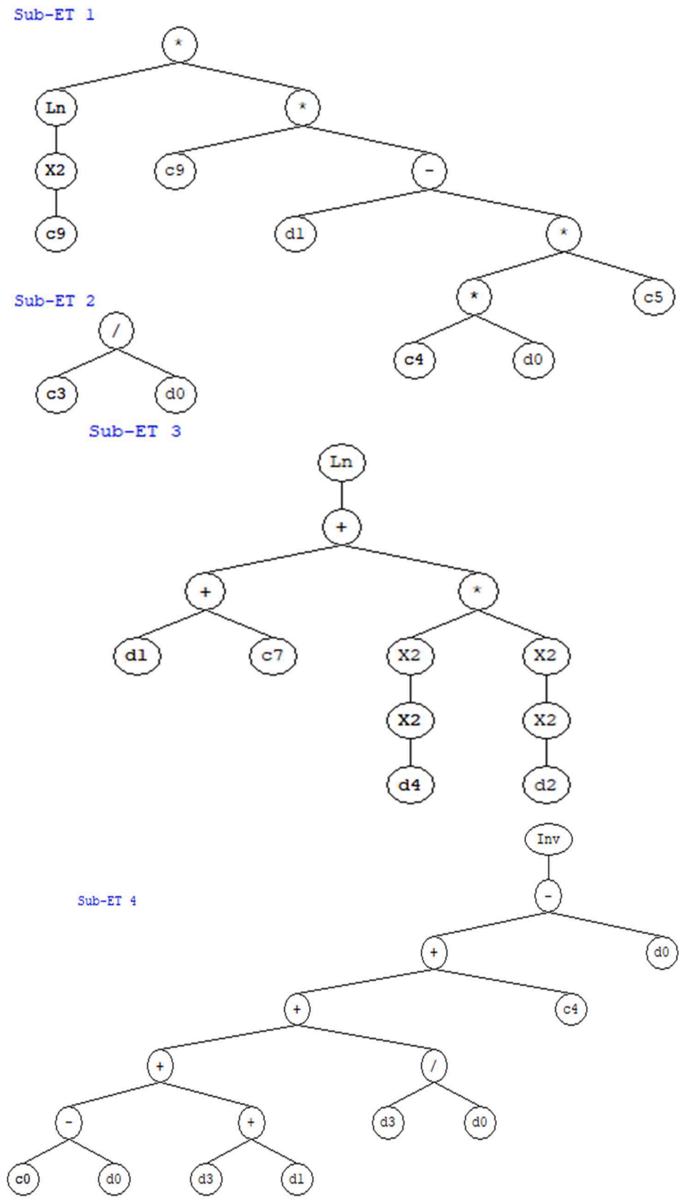

Fig. 8. Expression trees of the GEP algorithm.

MLR possesses a notable advantage in quantifying the impact of each variable [121]. However, MLR models are constrained to capturing linear relationships exclusively, necessitating the explicit inclusion of each variation or relationship as an input variable. This constraint limits the model's ability to generalize well, often oversimplifying the complexity of real-world scenarios. Fig. 14 compares the experimental and predicted values of the GEP, MEP, XGBoost, BES, and MLR models for predicting the CS of SFRC under elevated temperatures. In the validation set, the GEP model demonstrates markedly superior performance compared to the MLR model, showcasing a significantly higher R value (15.1 % increase) and markedly reduced values of RMSE (53.3 % decrease) and MAE (63.7 % decrease). Similarly, the MEP exhibits slightly higher R (8.3 % increase) and lower RMSE values (28.6 % decrease) than the MLR model during validation, albeit with a notable 42.6 % decrease in MAE. These outcomes underscore the limitations of the MLR model in precisely estimating the CS of SFRC under elevated temperatures.

4.3.2. Comparison of developed models and traditional design practice

Applying machine learning (ML) to forecast the strength of steel fiber-reinforced concrete provides notable benefits compared to conventional design methods. In the construction industry, design according to fire rating codes follows specific local and international standards that rely entirely on material type, not mixture properties. Purkiss [32] developed the first experimental table, the foundation for all these standards. His study presented the tabulated results of experiments on high-temperature concrete reinforced with steel fibers. Purkiss tested the specimens without fibers, samples with 0.75 % plain or looped fibers, and samples with 1.5 % plain fibers specimens to evaluate their residual compressive strength, flexural strength, dynamic modulus, and ultrasonic pulse velocity. The temperature range for the tests was 300–800 °C. It disclosed how temperature affected the material properties of SFRC, such as the amount of mix fibers, the change in residual stress, the loss of stiffness and tensile strength, the dynamic elastic modulus, and the ultrasonic pulse wave velocity of the affected material. However, the study contains numerous flaws. Firstly, the focus was solely on reducing material stiffness, neglecting other important properties such as material composition, fiber diameter, and type. The ML model differs from traditional methods by considering a more comprehensive range of material compositions and temperature conditions. This allows for more precise predictions based on data relevant to the environment. This leads to improved accuracy and reliability in assessing the structural integrity during fire exposure, ultimately assisting in creating safer and more resilient infrastructure designs. This developed ML surpasses the temperature limits (800 °C by Perkess) to 1200 °C and can also be extrapolated above. Furthermore, the reduction in strength in Perkess's study did not have any physical interpretation of numerical tabulated data, whereas this study yielded a proficient physical explanation of different parameters via SHAP analysis. The ML model provides a clear and comprehensible understanding of the impact of various material properties and high-temperature conditions on the strength of concrete through SHAP analysis. This enables more accurate identification of crucial parameters that influence fire resistance, providing valuable insights that conventional empirical approaches may fail to consider.

4.4. Model interpretability

4.4.1. SHAP global interpretation

In Fig. 15**,** the SHAP feature importance plot offers insights into the importance of different variables in predicting the desired output. Notably, it is evident that temperature has the highest importance in estimating the CS of SFRC exposed to high temperatures. Furthermore, when we focus on the characteristics associated with the fibers, it becomes evident that the diameter of the fibers (D) holds substantial importance in forecasting the CS of SFRC. This variable stands out with a notably higher contribution level compared to other fiber-related factors such as Vf and L. It can be confirmed from the resemblance to the diameter of steel in RC members where strength is reported more for high diameter than lower diameter. For the same reason, often heavily loaded RC members with greater depth utilize higher-diameter steel, ensuring durability demands. The heating rate contributes less to estimating the CS, as shown in Fig. 15. The low contribution of HR can also be noticed in Fig. 6. However, the temperatures exhibit a prominent mean SHAP value, surpassing the significance of the heating rate. This is evident from catastrophic events where consistent extreme temperatures resulted in concrete functional failure in comparatively less time. This indicates that temperature exerts a more substantial influence on the CS of SFRC than the heating rate.

Fig. 16 shows a SHAP summary plot that serves as a valuable tool for understanding how changes in input features impact the output, either positively or adversely. The ordinate plot organizes the variables in the rank of significance from highest to lowest, while the abscissa symbolizes specific SHAP values. The shade of the marks of the plot shows their extent, with blue dots indicative of smaller magnitudes and red dots demonstrating larger ones. Each mark in the plot relates to a sample in

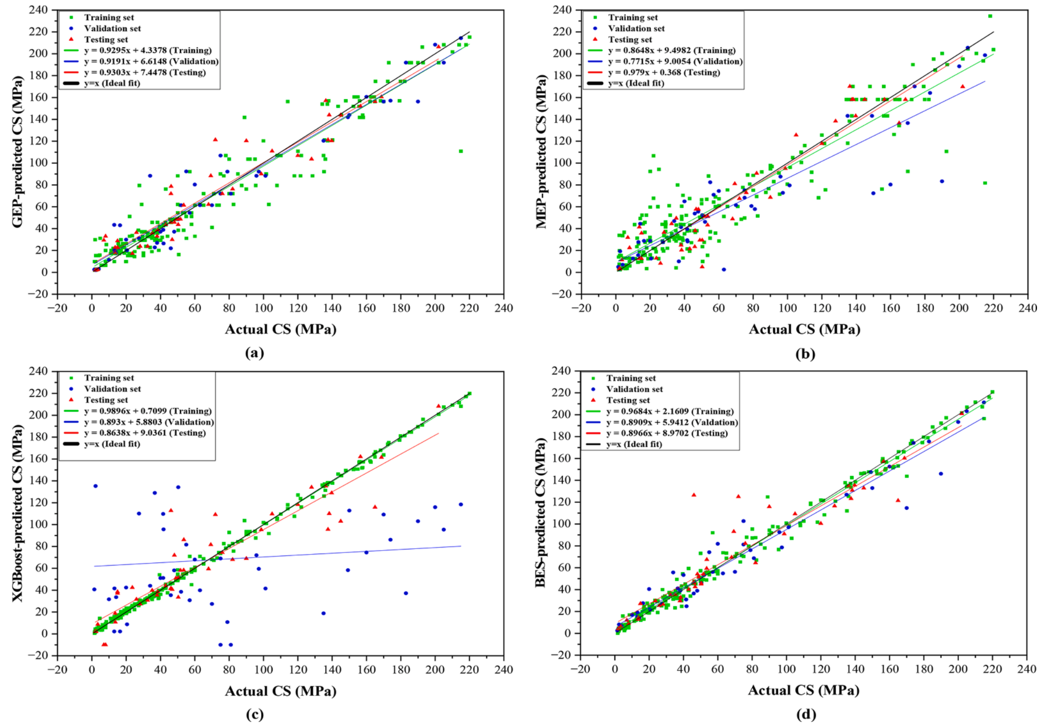

Fig. 9. Regression plot of GEP model.

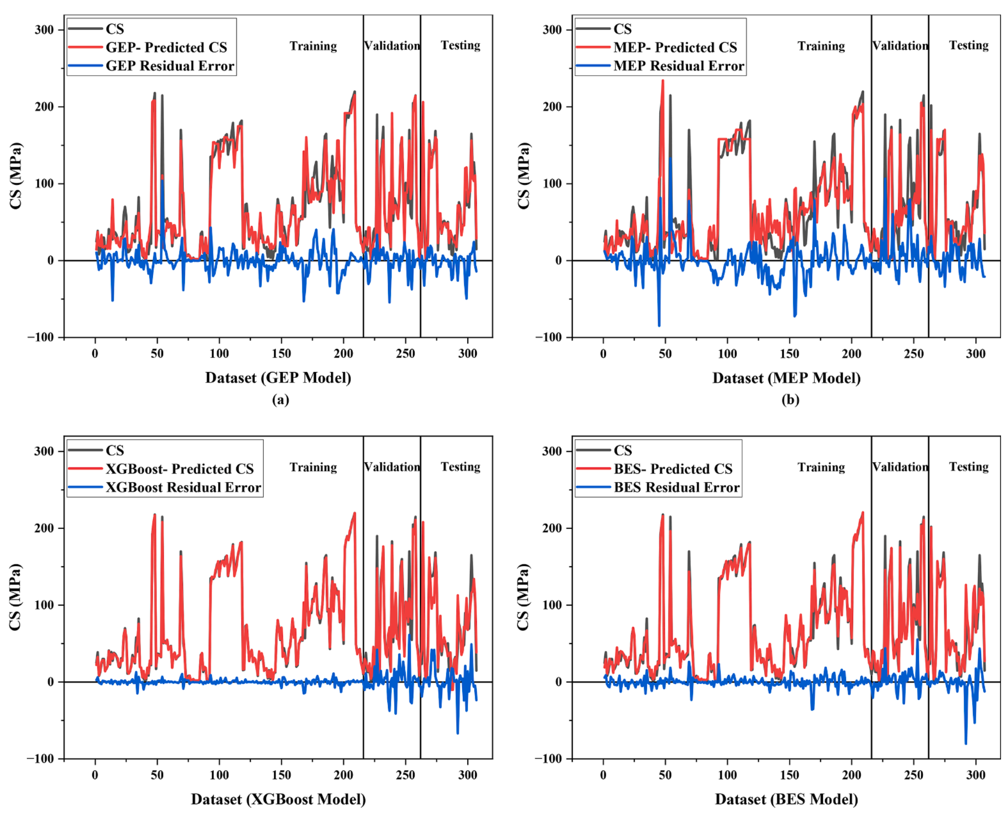

Fig. 10. Experimental vs. predicted values trend of the developed models.

the database. Remarkably, temperature emerges as a predominant factor influencing the strength of SFRC. An increase in temperature leads to a reduced CS and vice versa.

Similarly, a larger diameter negatively impacts the CS, as indicated by the red marks (high intensity) on the left side of the x-axis. In contrast, a higher dosage of fiber positively impacts the CS of SFRC subjected to elevated temperatures. Interestingly, the heating rate exhibits comparatively less influence on CS, implying that the concrete

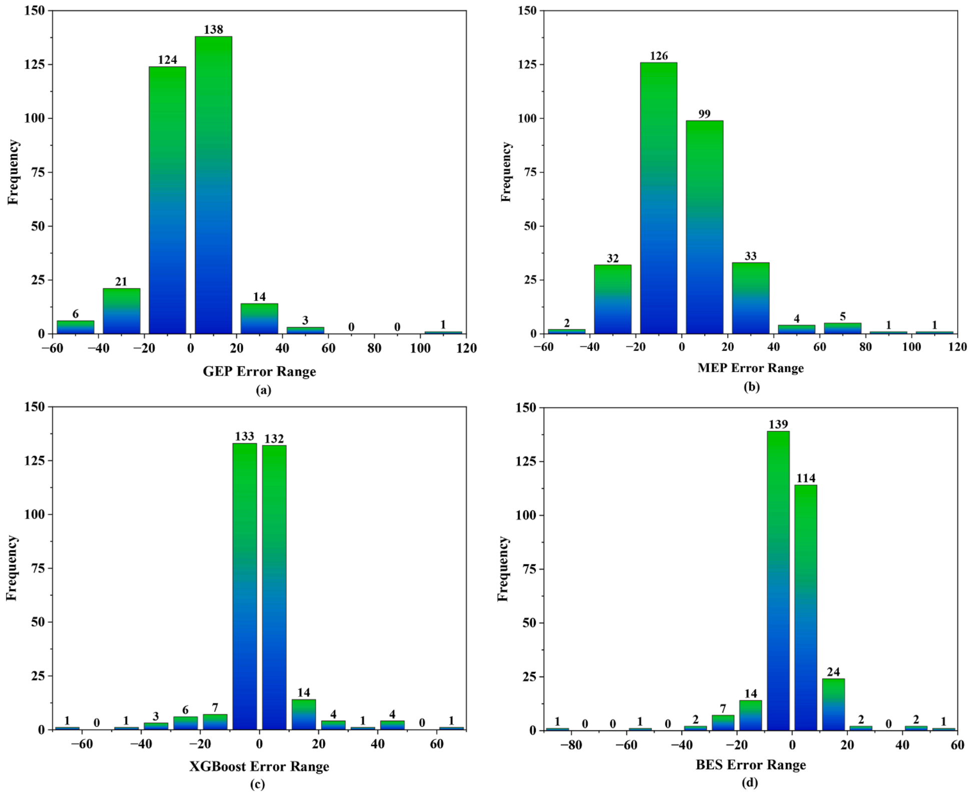

Fig. 11. Error histograms of the developed models.

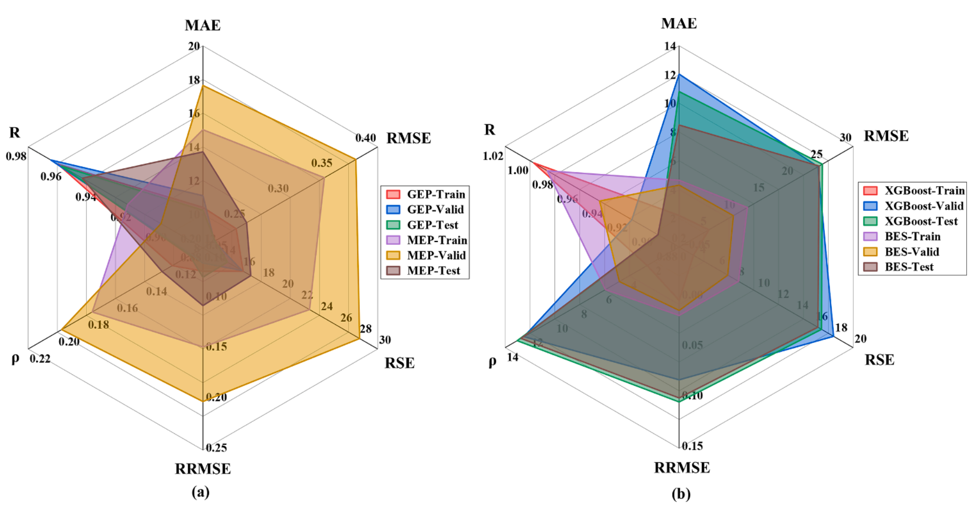

Fig. 12. Spider plot showing the statistical indicators of the models.

base temperature plays a more substantial role in predicting the target associated with the heating rate, which further opens an exciting topic to work on the durability and thermal stability of concrete concerning heat content and thermal absorption.

4.4.2. SHAP local interpretation

Global SHAP explanations show the importance of parameters and their effects on the output. However, to optimize input values, SHAP local interpretations are required. Fig. 17 SHAP feature interaction plots illustrate how features interact and impact the output. For instance, it shows that a temperature increase up to 300 °C does not lead to strength loss, but going beyond 300 °C significantly reduces compressive strength, as shown in Fig. 17(a). In previous studies, Tai et al. [78] found that SFRC exposed to temperatures between 200 °C and 300 °C exhibited no strength loss. However, a substantial, gradual loss in CS was observed once the temperature exceeded 400 °C [78].

Additionally, an observable enhancement in CS was noted as steel fibers' volume fraction (Vf) increased up to 1.5 %. Beyond this threshold, further V_f increments did not lead to increased CS, as shown in Fig. 17(b), aligning with findings from Ren et al. [122] reported that when V_f surpasses 1.5 %, the cement matrix is unable to fully encapsulate both the aggregate and steel fibers, resulting in reduced bonding between them. While different lengths of steel fibers have been tested in concrete, those falling within the range of 25 to 60 mm have shown a significant positive impact on compressive strength, as seen in Fig. 17 (c). Including steel fibers (SF) in the concrete mixture altered the

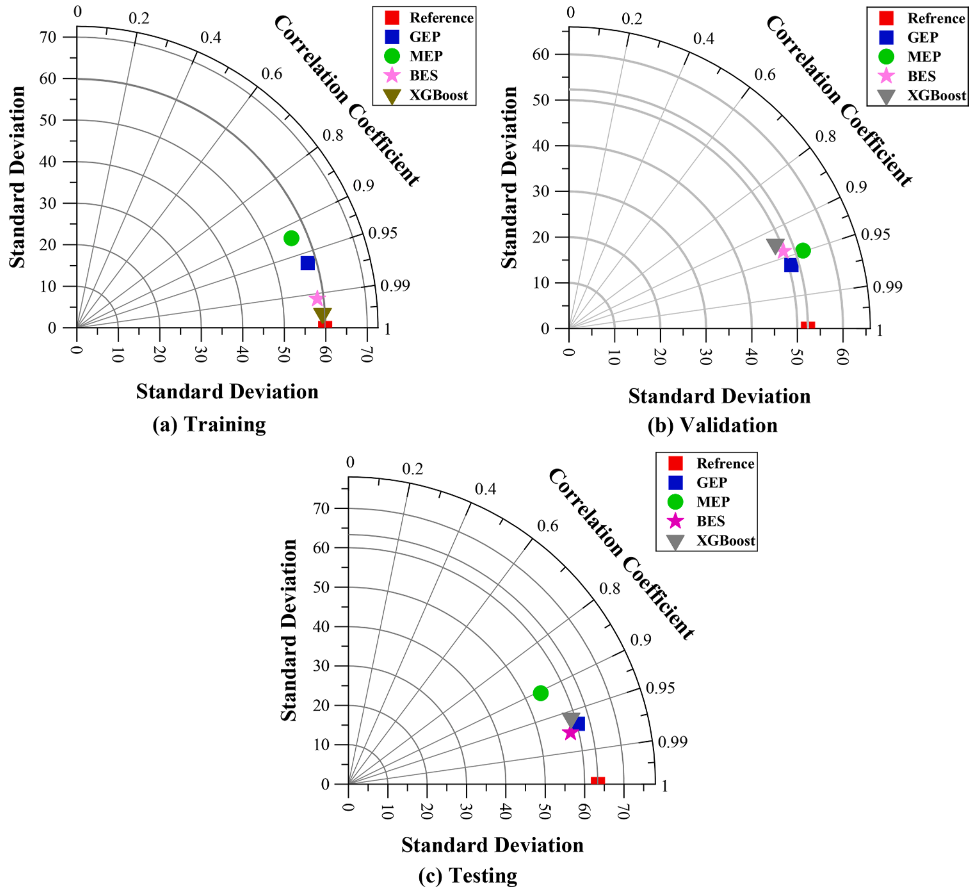

Fig. 13. Taylor diagrams: (a) Training, (b) Validation (c) Testing.

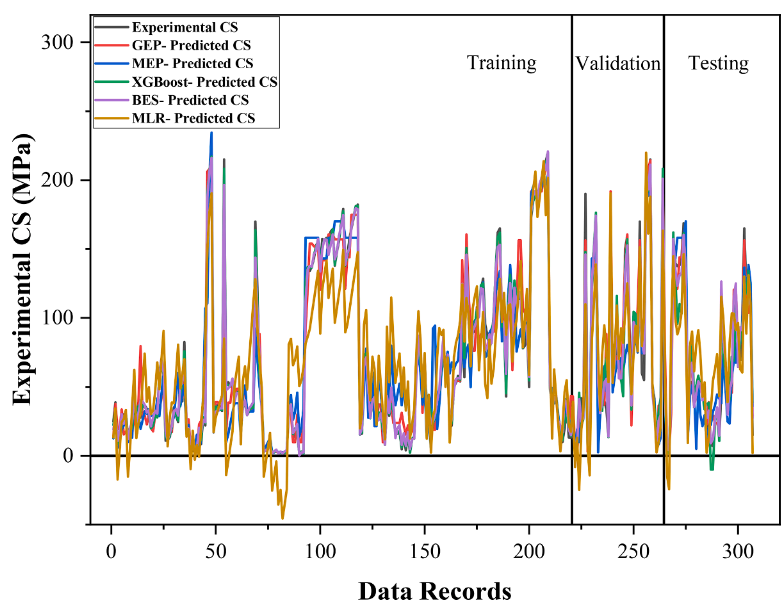

Fig. 14. MLR model comparison with ML models.

collapse mechanism from splitting to pullout, enhancing the bond strength for specimens that originally experienced splitting failure [123]. Similarly, fiber diameter values below 400 μm have been found to enhance compressive strength, whereas larger diameters have a detrimental effect, as indicated in Fig. 17(d). The heating rate's influence on strength is comparatively lower than that of the actual temperature, as illustrated in Fig. 17(e). This pattern is also reflected in Fig. 6, where a substantial negative correlation (-0.65) is observed between temperature and compressive strength, while the heating rate exhibits a less significant positive correlation (0.32). This underscores that the precise temperature of the test specimen holds greater importance in determining the CS, dominating the impact of the heating rate.

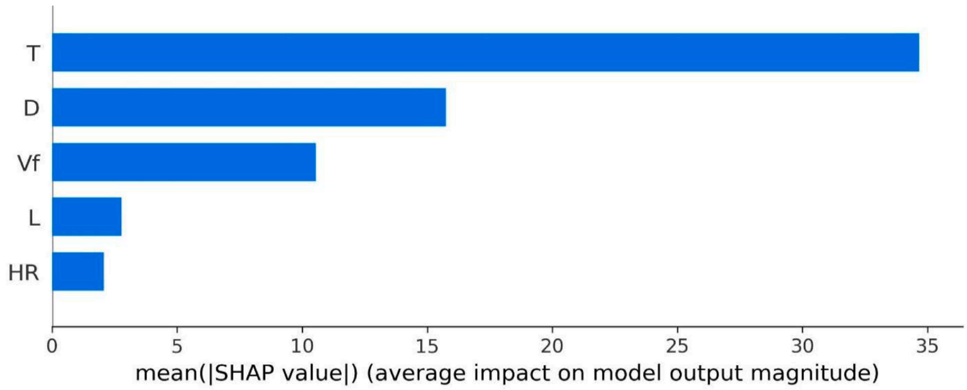

Fig. 15. SHAP features importance plot.

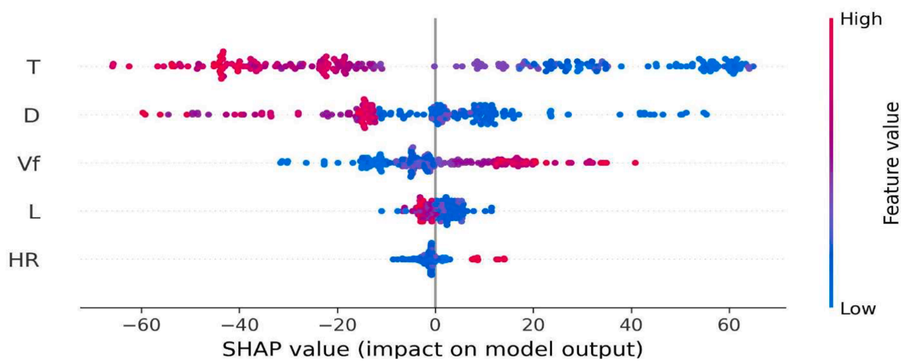

Fig. 16. SHAP feature influences the plot.

Furthermore, Fig. 18 presents two instances of local interpretation, which are specific predictions highlighted using the SHAP force diagram. In this diagram, the bolded value signifies the model's prediction at a particular point in the machine learning prediction process. The width of each feature's representation in the SHAP force plot directly corresponds to its impact on the output, with wider sections indicating stronger influences. The force diagram emphasizes that each variable possesses distinct impacts and interactions that collectively determine the outcomes at any given moment. For instance, in Fig. 18(a), it can be observed that at specific conditions, such as a temperature of 20 °C, a volume fraction of 2, and a fiber diameter of 200 mm, these variables exert a positive influence on the CS and result in enhanced CS of 155.53 MPa. Conversely, in Fig. 18(b), a scenario involving a temperature value of 750 °C results in a significantly adverse impact on compressive strength, ultimately leading to a reduced CS of (24.34 MPa). The SHAP force diagram provides valuable insights into how various parameter combinations affect the predicted outcomes in a specific condition.

In conclusion, SHAP provides broad and complex insights into specific cases with a comprehensive understanding of the model. SHAP analysis elucidated the internal functioning of the machine learning model, reducing the need for input from users. Consequently, it facilitates decision-making, even for those without technical proficiency. The local explanations effectively elucidate the reasoning behind forecasts. Furthermore, the SHAP interpretation aligns closely with the feature relationships identified during the data processing phase, as demonstrated in Fig. 6. Notably, volume fraction exhibits the highest positive correlation, registering at +0.49, while both temperature and fiber diameter display the most significant negative correlations, measuring -0.65 and -0.48, respectively, with CS. This interpretation affirms the validity of the decision-making processes employed in the GEP and MEP models, reinforcing their consistency with experimental observations.

Moreover, the SHAP interpretation goes beyond the correlation matrix's scope by determining each variable's interaction across the entire range. This depth of insight is a notable advantage over the correlation relationship plot, which offers a more limited perspective. Consequently, SHAP analysis provides a more comprehensive and nuanced understanding of the intricate relationships between the features and the response variable. As a result, SHAP analysis stands out as a reliable and powerful tool for unraveling the inner workings of machine learning models and elucidating the mechanisms behind their predictive outcomes.

4.5. Limitations of study and future work recommendations

The present work utilizes standalone machine learning techniques to forecast the compressive strength (CS) of SFRC. Future study has the potential to enhance forecasting accuracy by using hybrid machine-learning models. Support Vector Regression (SVR) optimization may be integrated with algorithms like the Grey Wolf Optimizer (GWO), Firefly Algorithm (FA), and Particle Swarm Optimizer (PSO) to enhance prediction optimization. By using this hybrid machine learning approach, it is possible to enhance the accuracy of SFRC CS predictions. In addition, although this study used the SHAP strategy to comprehend the models, future studies might acquire more insights by exploring other model-agnostic techniques such as LIME, Individual Conditional Expectations (ICE), and Partial Dependence Plot (PDP). Besides, doing a comparative examination of the outcomes obtained from various methodologies might enhance our understanding of model clarity alongside the insights gained via SHAP analysis. It is crucial to acknowledge the constraints of the investigation. The data source is derived from the existing literature, which presents variations in the experimental configurations among different research. It is recommended that future studies give more importance to conducting controlled experimental testing to enhance the resilience and

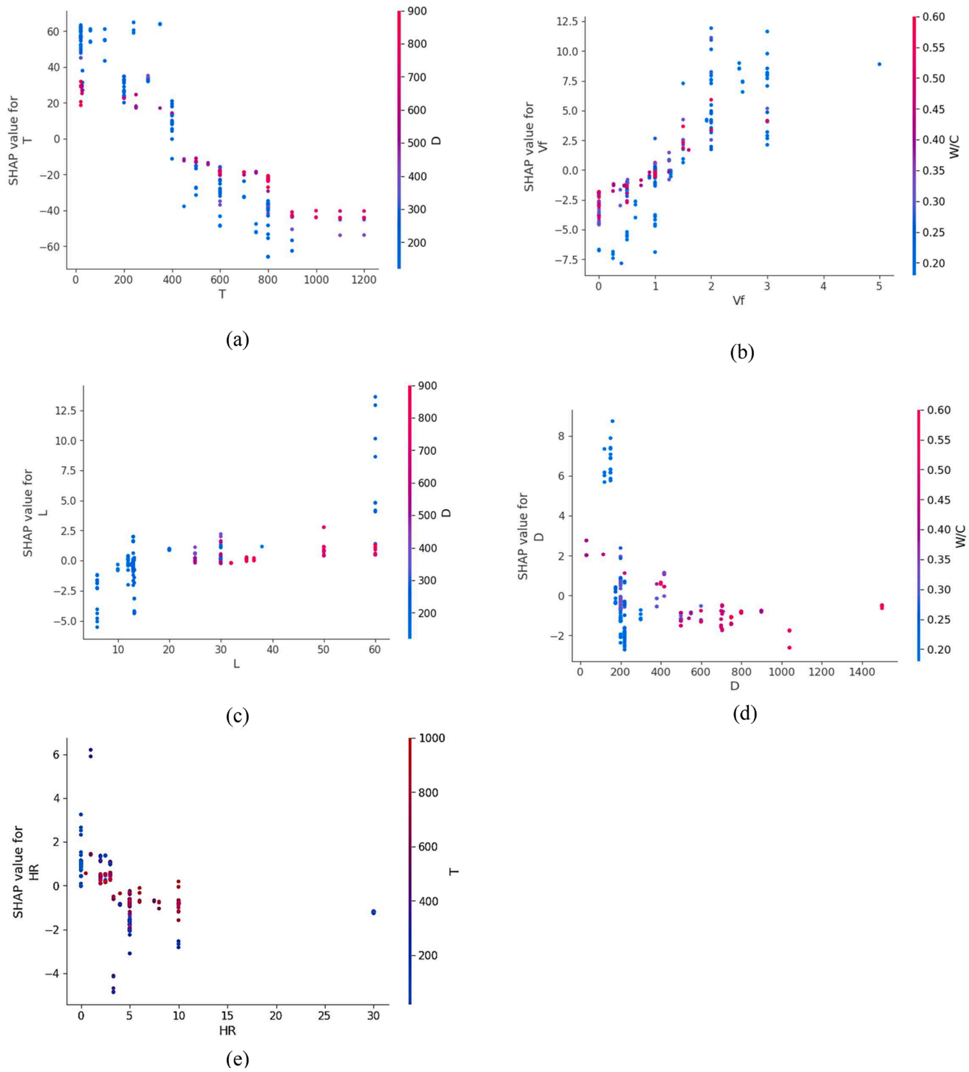

Fig. 17. SHAP dependence plot: (a) L, (b).

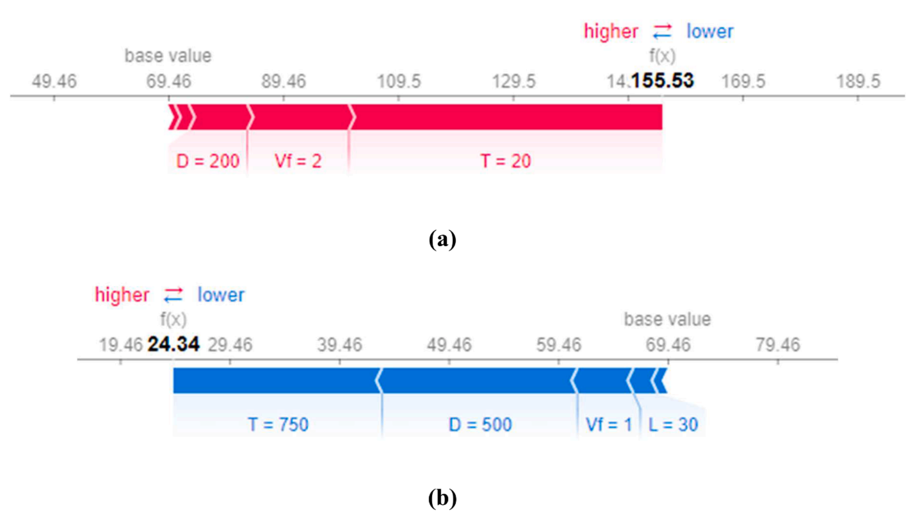

Fig. 18. SHAP force plots for selected prediction: (a) Instance I, (b) Instance II.

dependability of models. Collect data coming from a solitary and dependable source inside the same environment. This strategic approach provides a more secure foundation for predicting the compressive strength of SFRC. For a dataset with many variables and data records, it will not be feasible to apply independent and ensemble ML Models. Conventional ML models are unable to reach in-depth into the large dataset by connecting the PCAs of input variables with output variables. With synthetic data, the trends will be of more lengthy strings. Therefore, this study recommends Physics Informed Neural Networks (PINNs) to apply physics-based modeling equations, thereby creating deep data models with more real-time physical representation and prediction.

5. Conclusion

The present study utilized two distinct ML approaches, GEP and MEP, to predict the compressive strength of SFRC under elevated temperatures. A dataset comprising 307 samples from 44 published experimental trials was employed for training and validating the machine learning models, with 70 % dedicated to training and 30 % to validation. SHAP was employed to provide insights into the model predictions locally and globally. The following highlights key findings from the study:

1. The GEP model exhibited outstanding predictive accuracy, with R-values of 0.963, 0.967, and 0.961 for training, validation, and testing, respectively, highlighting its reliable performance in predicting SFRC strength under elevated temperatures. On the other hand, the MEP model displayed moderate accuracy, achieving R-values of 0.923, 0.904, and 0.949 across the same phases. Although both the XGBoost and BES models performed strongly during training, their accuracy decreased during the validation and testing stages.
2. Empirical formulation has been developed based on GEP to estimate the strength of SFRC exposed to high temperatures, offering a simplified mathematical equation for adequate estimation of compressive strength.
3. This study considered temperature and heating rate as input factors. The SHAP analysis indicated that temperature significantly impacted the CS of SFRC. On the other hand, it was revealed that the heating rate had a negligible influence on the strength. Furthermore, increasing the fiber dosage up to 1.5 % results in a substantial gain in compressive strength, but no further improvement is found beyond this threshold.

The study utilized a dataset of 307 samples for ML model development, suggesting that a more extensive dataset could improve model robustness. While the focus was on individual models, future exploration of hybrid models (XGBoost-SVR, RF-SVR, neural network-SVR, and XGBoost-CNN) is recommended for predicting SFRC characteristics at high temperatures. Additionally, alternative model interpretation techniques, such as LIME, PDP, and ICE, could be considered in future studies. Further research opportunities include developing ML-based models for predicting the strength characteristics of hybrid fiber-reinforced concrete at high temperatures.

CRediT authorship contribution statement

Mohsin Ali: Writing – original draft, Software, Methodology, Conceptualization. **Li Chen:** Supervision, Conceptualization. **Qadir Bux Alias Imran Latif Qureshi:** Software. **Deema Mohammed Alsekait:** Data curation. **Adil Khan:** Formal analysis. **Kiran Arif:** Visualization. **Muhammad Luqman:** Writing – review & editing. **Diaa Salama Abd Elminaam:** Resources. **Amir Hamza:** Writing – review & editing. **Majid Khan:** Validation.

Declaration of competing interest

The authors declare that they have no known competing financial interests or personal relationships that could have appeared to influence the work reported in this paper.

Acknowledgment

The authors would like to acknowledge the support of Princess Nourah bint Abdulrahman University Researchers Supporting Project number (PNURSP2024R435), Princess Nourah bint Abdulrahman University, Riyadh, Saudi Arabia.

Data availability

Data will be made available on request.

References

[1] S.S. Pakzad, N. Roshan, M. Ghalehnovi, Comparison of various machine learning algorithms used for compressive strength prediction of steel fiber-reinforced concrete, Sci. Rep. 13 (1) (2023), https://doi.org/10.1038/s41598-023-30606-y.
[2] “Concrete Under Severe Conditions. INTERNATIONAL CONFERENCE. 7TH . (CONSEC13) (3 VOLS) ENVIRONMENT AND LOADING - proceedings.com,” Curran Associates, Inc. [Online], 2013. Available: https://www.proceedings.com/30521.html.
[3] M.V. Mohod, Performance of steel fiber reinforced concrete, Res. Inventy Int. J. Eng. Sci. 1 (2012) 1–04. Accessed: Aug. 24, 2024. [Online]. Available: www.researchinventy.com.
[4] L. Sabat, S.S. Pradhan, Experimental evaluation of a composite material using GFRC, in: Materials Today: Proceedings, 2020, https://doi.org/10.1016/j.matpr.2020.01.170.
[5] S. Kakooei, H.M. Akil, M. Jamshidi, J. Rouhi, The effects of polypropylene fibers on the properties of reinforced concrete structures, Constr. Build. Mater. 27 (1) (2012), https://doi.org/10.1016/j.conbuildmat.2011.08.015.
[6] M. Daneshfar, A. Hassani, M.R.M. Aliha, F. Berto, Evaluating mechanical properties of macro-synthetic fiber-reinforced concrete with various types and contents, Strength Mater. 49 (5) (2017), https://doi.org/10.1007/s11223-017-9907-z.
[7] M.I. Khan, M. Umair, K. Shaker, A. Basit, Y. Nawab, M. Kashif, Impact of waste fibers on the mechanical performance of concrete composites, J. Textile Instit. 111 (11) (2020), https://doi.org/10.1080/00405000.2020.1736423.
[8] H. Zhou, B. Jia, H. Huang, Y. Mou, Experimental study on basic mechanical properties of basalt fiber reinforced concrete, Materials (Basel) 13 (6) (2020), https://doi.org/10.3390/ma13061362.
[9] T. Shafighfard, E. Demir, M. Yildiz, Design of fiber-reinforced variable-stiffness composites for different open-hole geometries with fiber continuity and curvature constraints, Compos. Struct. 226 (2019) 111280, https://doi.org/10.1016/j.compstruct.2019.111280. Oct.
[10] T. Shafighfard, T.A. Cender, E. Demir, Additive manufacturing of compliance optimized variable stiffness composites through short fiber alignment along curvilinear paths, Addit. Manuf. 37 (2021) 101728, https://doi.org/10.1016/j.addma.2020.101728. Jan.
[11] T. Shafighfard, M. Mieloszyk, Experimental and numerical study of the additively manufactured carbon fibre reinforced polymers including fibre Bragg grating sensors, Compos. Struct. 299 (2022) 116027, https://doi.org/10.1016/j.compstruct.2022.116027. Nov.
[12] M. Khan, M. Cao, C. Xie, M. Ali, Effectiveness of hybrid steel-basalt fiber reinforced concrete under compression, Case Stud. Constr. Mater. 16 (2022) e00941, https://doi.org/10.1016/j.cscm.2022.e00941. Jun.
[13] M. Khan, M. Cao, S.H. Chu, M. Ali, Properties of hybrid steel-basalt fiber reinforced concrete exposed to different surrounding conditions, Constr. Build. Mater. 322 (2022) 126340, https://doi.org/10.1016/j.conbuildmat.2022.126340. Mar.
[14] C. L. L, K.M Cao, M. Xie, The relationship between reinforcing index and flexural parameters of new hybrid fiber reinforced slab Comput. Concr (2018) 481–492.
[15] M. Cao, M. Khan, Effectiveness of multiscale hybrid fiber reinforced cementitious composites under single degree of freedom hydraulic shaking table, Struct. Concr. 22 (1) (2021) 535–549, https://doi.org/10.1002/suco.201900228. Feb.
[16] B. Ali, Development of environment-friendly and ductile recycled aggregate concrete through synergetic use of hybrid fibers, Environ. Sci. Pollut. Res. 29 (23) (2022) 34452–34463, https://doi.org/10.1007/s11356-022-18627-y. May.
[17] H. Jamal, et al., Analysis of viscoelastic behaviour in asphalt pavement through four-point beam bending tests, Budownictwo i Architektura 23 (2) (2024) 059–072, https://doi.org/10.35784/BUD-ARCH.5501. Jun.
[18] M.F. Javed, B. Siddiq, K. Onyelowe, W.A. Khan, M. Khan, Metaheuristic optimization algorithms-based prediction modeling for titanium dioxide-Assisted photocatalytic degradation of air contaminants, Results. Eng. 23 (2024) 102637, https://doi.org/10.1016/J.RINENG.2024.102637. Sep.
[19] U. Asif, M.F. Javed, M. Abuhussain, M. Ali, W.A. Khan, A. Mohamed, Predicting the mechanical properties of plastic concrete: an optimization method by using genetic programming and ensemble learners, Case Stud. Constr. Mater. 20 (2024) e03135, https://doi.org/10.1016/J.CSCM.2024.E03135. Jul.
[20] Ş. Yazıcı, G. İnan, V. Tabak, Effect of aspect ratio and volume fraction of steel fiber on the mechanical properties of SFRC, Constr. Build. Mater. 21 (6) (2007) 1250–1253, https://doi.org/10.1016/j.conbuildmat.2006.05.025. Jun.

[21] M. Ahmad, et al., Supervised learning methods for modeling concrete compressive strength prediction at high temperature, Materials (Basel) 14 (8) (2021), https://doi.org/10.3390/ma14081983.
[22] J.L. Gross, L.T. Phan, Summary of best practice guidelines for structural fire resistance design of concrete and steel buildings, Struct. Congr. (2010) 2010, https://doi.org/10.1061/41130(369)215.
[23] I. Janotka, L. Bágel, Pore structures, permeabilities, and compressive strengths of concrete at temperatures up to 800°C, ACI. Mater. J. 99 (2) (2002), https://doi.org/10.14359/11713.
[24] G.F. Peng, W.W. Yang, J. Zhao, Y.F. Liu, S.H. Bian, L.H. Zhao, Explosive spalling and residual mechanical properties of fiber-toughened high-performance concrete subjected to high temperatures, Cem. Concr. Res. 36 (4) (2006), https://doi.org/10.1016/j.cemconres.2005.12.014.
[25] Q. Ma, R. Guo, Z. Zhao, Z. Lin, and K. He, "Mechanical properties of concrete at high temperature-a review," 2015. doi: 10.1016/j.conbuildmat.2015.05.131.
[26] W. Zhu, M.A. Rahman, M. Moomen, W.A. Khan, J. Codjoe, An analysis of the impact of injury severity on incident clearance time on urban interstates using a bivariate random-parameter probit model, Stats. (Basel) 7 (2024) 863–874, https://doi.org/10.3390/STATS7030052. *Pages*vol. 7, no. 3, pp. 863–874, Aug. 2024.
[27] B. Ali, P. Li, D. Khan, M.R.M. Hasan, W.A. Khan, Investigation into the effect of waste engine oil and vegetable oil recycling agents on the performance of laboratory-aged bitumen, Budownictwo i Architektura 23 (1) (2024) 033–054, https://doi.org/10.35784/BUD-ARCH.5500. Mar.
[28] H. Wu, X. Lin, A. Zhou, A review of mechanical properties of fibre reinforced concrete at elevated temperatures, Cem. Concr. Res. 135 (2020) 106117, https://doi.org/10.1016/j.cemconres.2020.106117. Sep.
[29] D. Gao, D. Yan, X. Li, Splitting strength of GGBFS concrete incorporating with steel fiber and polypropylene fiber after exposure to elevated temperatures, Fire Saf. J. (2012), https://doi.org/10.1016/j.firesaf.2012.07.009.
[30] C.S. Poon, Z.H. Shui, L. Lam, H. Fok, S.C. Kou, Influence of moisture states of natural and recycled aggregates on the slump and compressive strength of concrete, Cem. Concr. Res. 34 (1) (2004), https://doi.org/10.1016/S0008-8846(03)00186-8.
[31] F.E. Jalal, M. Iqbal, W.A. Khan, A. Jamal, K. Onyelowe, Lekhraj, ANN-based swarm intelligence for predicting expansive soil swell pressure and compression strength, Sci. Rep. 14 (1) (2024) 1–34, https://doi.org/10.1038/s41598-024-65547-7. *14:1*Jun. 2024.
[32] J.A. Purkiss, Steel fibre reinforced concrete at elevated temperatures, Int. J. Cement Compos. Lightweight Concr. 6 (3) (1984), https://doi.org/10.1016/0262-5075(84)90006-X.
[33] R. Ismail, F.A.A. Zakwan, C. Petrus, N.A. Marzuki, N.H. Hashim, M.F. Mustafa, Compressive behavior of steel fiber reinforced concrete after exposed to high temperatures, InCIEC (2013) 731–740, https://doi.org/10.1007/978-981-4585-02-6_63, 2014.
[34] A. Lau, M. Anson, Effect of high temperatures on high performance steel fibre reinforced concrete, Cem. Concr. Res. 36 (9) (2006), https://doi.org/10.1016/j.cemconres.2006.03.024.
[35] J.F. Dong, Q.Y. Wang, Z.W. Guan, H.K. Chai, High-temperature behaviour of basalt fibre reinforced concrete made with recycled aggregates from earthquake waste, J. Build. Eng. 48 (2022) 103895, https://doi.org/10.1016/j.jobe.2021.103895. May.
[36] Q. Li, M. Wang, H. Sun, G. Yu, Effect of heating rate on the free expansion deformation of concrete during the heating process, J. Build. Eng. 34 (2021) 101896, https://doi.org/10.1016/J.JOBE.2020.101896. Feb.
[37] Z. Zhang, Z. Zhang, F. Di Caprio, G.X. Gu, Machine learning for accelerating the design process of double-double composite structures, Compos. Struct. 285 (2022) 115233, https://doi.org/10.1016/j.compstruct.2022.115233. Apr.
[38] L. Chen, et al., Development of predictive models for sustainable concrete via genetic programming-based algorithms, J. Mater. Res. Technol. 24 (2023), https://doi.org/10.1016/j.jmrt.2023.04.180.
[39] I. Ilyas, et al., Advanced machine learning modeling approach for prediction of compressive strength of FRP confined concrete using multiphysics genetic expression programming, Polymers 2022 14 (2022) 1789, https://doi.org/10.3390/POLYM14091789. *Page*vol. 14, no. 9, p. 1789, Apr.
[40] I. Ilyas, et al., Forecasting strength of CFRP confined concrete using multi expression programming, Materials (Basel) 14 (2021) 7134, https://doi.org/10.3390/MA14237134. *Page*vol. 14, no. 23, p. 7134, Nov. 2021.
[41] C. Chen, G.X. Gu, Generative deep neural networks for inverse materials design using backpropagation and active learning, Adv. Sci. 7 (5) (Mar. 2020) 1902607, https://doi.org/10.1002/advs.201902607.
[42] R. Solhmirzaei, H. Salehi, V. Kodur, M.Z. Naser, Machine learning framework for predicting failure mode and shear capacity of ultra high performance concrete beams, Eng. Struct. 224 (2020), https://doi.org/10.1016/j.engstruct.2020.111221.
[43] M. Shang, et al., Predicting the mechanical properties of RCA-based concrete using supervised machine learning algorithms, Materials (Basel) 15 (2) (2022), https://doi.org/10.3390/ma15020647.
[44] M. Nematzadeh, A.A. Shahmansouri, M. Fakoor, Post-fire compressive strength of recycled PET aggregate concrete reinforced with steel fibers: optimization and prediction via RSM and GEP, Constr. Build. Mater. 252 (2020), https://doi.org/10.1016/j.conbuildmat.2020.119057.
[45] Y. Huang, J. Zhang, F.Tze Ann, G. Ma, Intelligent mixture design of steel fibre reinforced concrete using a support vector regression and firefly algorithm based multi-objective optimization model, Constr. Build. Mater. 260 (2020) 120457, https://doi.org/10.1016/j.conbuildmat.2020.120457. Nov.
[46] J. Sun, Y. Ma, J. Li, J. Zhang, Z. Ren, X. Wang, Machine learning-aided design and prediction of cementitious composites containing graphite and slag powder, J. Build. Eng. 43 (2021) 102544, https://doi.org/10.1016/j.jobe.2021.102544. Nov.
[47] A. Ashrafian, A.A. Shahmansouri, H.Akbarzadeh Bengar, A. Behnood, Post-fire behavior evaluation of concrete mixtures containing natural zeolite using a novel metaheuristic-based machine learning method, Arch. Civil Mech. Eng. 22 (2) (2022), https://doi.org/10.1007/s43452-022-00415-7.
[48] A. Memarzadeh, A.A. Shahmansouri, K. Poologanathan, A novel prediction model for post-fire elastic modulus of circular recycled aggregate concrete-filled steel tubular stub columns, Steel Compos. Struct. 44 (3) (2022), https://doi.org/10.12989/scs.2022.44.3.309.
[49] M.K. Almustafa, M.L. Nehdi, Machine learning prediction of structural response of steel fiber-reinforced concrete beams subjected to far-field blast loading, Cem. Concr. Compos. 126 (2022) 104378, https://doi.org/10.1016/j.cemconcomp.2021.104378. Feb.
[50] H. Chen, J. Yang, X. Chen, A convolution-based deep learning approach for estimating compressive strength of fiber reinforced concrete at elevated temperatures, Constr. Build. Mater. 313 (2021) 125437, https://doi.org/10.1016/j.conbuildmat.2021.125437. Dec.
[51] M.X. Xiong, J.Y. Richard Liew, Spalling behavior and residual resistance of fibre reinforced Ultra-High performance concrete after exposure to high temperatures, Materiales de Construccion 65 (320) (2015), https://doi.org/10.3989/mc.2015.00715.
[52] T. Shafighfard, F. Bagherzadeh, R.A. Rizi, D.Y. Yoo, Data-driven compressive strength prediction of steel fiber reinforced concrete (SFRC) subjected to elevated temperatures using stacked machine learning algorithms, J. Mater. Res. Technol. 21 (2022), https://doi.org/10.1016/j.jmrt.2022.10.153.
[53] R. Alyousef, et al., Machine learning-driven predictive models for compressive strength of steel fiber reinforced concrete subjected to high temperatures, Case Stud. Constr. Mater. 19 (2023), https://doi.org/10.1016/j.cscm.2023.e02418.
[54] J.R. Koza, Genetic Programming: On the Programming of Computers by Means of Natural Selection, MIT Press, Cambridge, MA, 1992. ISBN 0-262-11170-5.
[55] P.A. Pattanaik, T. Swarnkar, Vision-based malaria parasite image analysis: a systematic review, Int. J. Bioinform. Res. Appl. 15 (1) (2019) 1, https://doi.org/10.1504/IJBRA.2019.097987.
[56] P. Sarir, J. Chen, P.G. Asteris, D.J. Armaghani, M.M. Tahir, Developing GEP tree-based, neuro-swarm, and whale optimization models for evaluation of bearing capacity of concrete-filled steel tube columns, Eng. Comput. 37 (1) (2021) 1–19, https://doi.org/10.1007/s00366-019-00808-y. Jan.
[57] Mihai Oltean, Dumitrescu, Multi Expression Programming, Mihai Oltean Department of Computer Science Babe¸s-Bolyai University Kogalniceanu 1 Cluj-Napoca, Romania, 2002.
[58] T. Chen, C. Guestrin, XGBoost: a scalable tree boosting system, in: Proceedings of the ACM SIGKDD International Conference on Knowledge Discovery and Data Mining 13-17-August-2016, 2016, pp. 785–794, https://doi.org/10.1145/2939672.2939785/SUPPL_FILE/KDD2016_CHEN_BOOSTING_SYSTEM_01-ACM.MP4. Aug.
[59] J.H. Friedman, "Greedy function approximation: a gradient boosting machine.," https://doi.org/10.1214/aos/1013203451, vol. 29, no. 5, pp. 1189–1232, Oct. 2001, doi: 10.1214/aos/1013203451.
[60] D. Nielsen, "Tree boosting with XGBoost - why does XGBoost win 'every' machine learning competition?," 2016, Accessed: Sep. 16, 2024. [Online]. Available: https://ntnuopen.ntnu.no/ntnu-xmlui/handle/11250/2433761.
[61] B. Mihaljević, C. Bielza, P. Larrañaga, Bayesian networks for interpretable machine learning and optimization, Neurocomputing. 456 (2021) 648–665, https://doi.org/10.1016/J.NEUCOM.2021.01.138. Oct.
[62] M. Abdar, et al., A review of uncertainty quantification in deep learning: techniques, applications and challenges, Inform. Fusion 76 (2021) 243–297, https://doi.org/10.1016/j.inffus.2021.05.008. Dec.
[63] R. Martin, N. Syring, Direct Gibbs posterior inference on risk minimizers: construction, concentration, and calibration, Handbook Stat. 47 (2022) 1–41, https://doi.org/10.1016/BS.HOST.2022.06.004. Jan.
[64] H. Feng, L. Li, W. Wang, Z. Cheng, D. Gao, Mechanical properties of high ductility hybrid fibres reinforced magnesium phosphate cement-based composites, Compos. Struct. 284 (2022), https://doi.org/10.1016/j.compstruct.2022.115219.
[65] Y.N. Chan, X. Luo, W. Sun, Compressive strength and pore structure of high-performance concrete after exposure to high temperature up to 800°C, Cem. Concr. Res. 30 (2) (2000), https://doi.org/10.1016/S0008-8846(99)00240-9.
[66] G.M. Chen, Y.H. He, H. Yang, J.F. Chen, Y.C. Guo, Compressive behavior of steel fiber reinforced recycled aggregate concrete after exposure to elevated temperatures, Constr. Build. Mater. 71 (2014), https://doi.org/10.1016/j.conbuildmat.2014.08.012.
[67] F.U.A. Shaikh, A. Hosan, Mechanical properties of steel fibre reinforced geopolymer concretes at elevated temperatures, Constr. Build. Mater. 114 (2016), https://doi.org/10.1016/j.conbuildmat.2016.03.158.
[68] F. Aslani, J. Kelin, Assessment and development of high-performance fibre-reinforced lightweight self-compacting concrete including recycled crumb rubber aggregates exposed to elevated temperatures, J. Clean. Prod. 200 (2018), https://doi.org/10.1016/j.jclepro.2018.07.323.
[69] Y.N. Kumar, B.Dean Kumar, B.L.P. Swami, Mechanical properties of geopolymer concrete reinforced with steel and glass fibers with various mineral admixtures, in: Materials Today: Proceedings, 2022, https://doi.org/10.1016/j.matpr.2021.10.050.

[70] J. Ran, T. Li, D. Chen, L. Shang, W. Li, Q. Zhu, Mechanical properties of concrete reinforced with corrugated steel fiber under uniaxial compression and tension, Structures 34 (2021), https://doi.org/10.1016/j.istruc.2021.08.135.

[71] C.S. Poon, Z.H. Shui, L. Lam, Compressive behavior of fiber reinforced high-performance concrete subjected to elevated temperatures, Cem. Concr. Res. 34 (12) (2004), https://doi.org/10.1016/j.cemconres.2004.02.011.

[72] P.K. Prasanna, K. Srinivasu, A.Ramachandra Murthy, Strength and durability of fiber reinforced concrete with partial replacement of cement by ground granulated blast furnace slag, in: Materials Today: Proceedings, 2021, https://doi.org/10.1016/j.matpr.2021.06.267.

[73] K.K. Sideris, P. Manita, E. Chaniotakis, Performance of thermally damaged fibre reinforced concretes, Constr. Build. Mater. 23 (3) (2009), https://doi.org/10.1016/j.conbuildmat.2008.08.009.

[74] A.A. Deshpande, D. Kumar, R. Ranade, Influence of high temperatures on the residual mechanical properties of a hybrid fiber-reinforced strain-hardening cementitious composite, Constr. Build. Mater. 208 (2019), https://doi.org/10.1016/j.conbuildmat.2019.02.129.

[75] R.R. Agra, R. Serafini, A.D. de Figueiredo, Effect of high temperature on the mechanical properties of concrete reinforced with different fiber contents, Constr. Build. Mater. 301 (2021), https://doi.org/10.1016/j.conbuildmat.2021.124242.

[76] M. Chen, H. Si, X. Fan, Y. Xuan, M. Zhang, Dynamic compressive behaviour of recycled tyre steel fibre reinforced concrete, Constr. Build. Mater. 316 (2022), https://doi.org/10.1016/j.conbuildmat.2021.125896.

[77] M. Ozawa, S. Subedi Parajuli, Y. Uchida, B. Zhou, Preventive effects of polypropylene and jute fibers on spalling of UHPC at high temperatures in combination with waste porous ceramic fine aggregate as an internal curing material, Constr. Build. Mater. 206 (2019), https://doi.org/10.1016/j.conbuildmat.2019.02.056.

[78] Y.S. Tai, H.H. Pan, Y.N. Kung, Mechanical properties of steel fiber reinforced reactive powder concrete following exposure to high temperature reaching 800 °c, Nuclear Eng. Design 241 (7) (2011), https://doi.org/10.1016/j.nucengdes.2011.04.008.

[79] C.K. Mahapatra, S.V. Barai, Temperature impact on residual properties of self-compacting based hybrid fiber reinforced concrete with fly ash and colloidal nano silica, Constr. Build. Mater. 198 (2019), https://doi.org/10.1016/j.conbuildmat.2018.11.155.

[80] A. Krishna, S.R.M. Kaliyaperumal, Effect of elevated temperature on strength and ductility of axially loaded hybrid fiber reinforced concrete columns, Structures 34 (2021), https://doi.org/10.1016/j.istruc.2021.09.099.

[81] W. Khalil, Influence of high temperature on steel fiber reinforced concrete, J. Eng. Sustain. Develop. 10 (2008).

[82] K. Yang, Z. Tang, Z. Cheng, H. Zhao, R. Feng, G. Long, Mechanical properties of ultra-high strength cement-based materials (UHSC) incorporating metal powders and steel fibers, Constr. Build. Mater. 318 (2022), https://doi.org/10.1016/j.conbuildmat.2021.125926.

[83] L. Li, R. Zhang, L. Jin, X. Du, J. Wu, W. Duan, Experimental study on dynamic compressive behavior of steel fiber reinforced concrete at elevated temperatures, Constr. Build. Mater. 210 (2019), https://doi.org/10.1016/j.conbuildmat.2019.03.138.

[84] H. Caetano, G. Ferreira, J.P.C. Rodrigues, P. Pimienta, Effect of the high temperatures on the microstructure and compressive strength of high strength fibre concretes, Constr. Build. Mater. 199 (2019), https://doi.org/10.1016/j.conbuildmat.2018.12.074.

[85] N. Yermak, P. Pliya, A.L. Beaucour, A. Simon, A. Noumowé, Influence of steel and/or polypropylene fibres on the behaviour of concrete at high temperature: spalling, transfer and mechanical properties, Constr. Build. Mater. 132 (2017), https://doi.org/10.1016/j.conbuildmat.2016.11.120.

[86] W. Khaliq, V. Kodur, Thermal and mechanical properties of fiber reinforced high performance self-consolidating concrete at elevated temperatures, Cem. Concr. Res. 41 (11) (2011), https://doi.org/10.1016/j.cemconres.2011.06.012.

[87] A. Karimi, M. Nematzadeh, Axial compressive performance of steel tube columns filled with steel fiber-reinforced high strength concrete containing tire aggregate after exposure to high temperatures, Eng. Struct. 219 (2020), https://doi.org/10.1016/j.engstruct.2020.110608.

[88] W. Zheng, H. Li, Y. Wang, Compressive stress-strain relationship of steel fiber-reinforced reactive powder concrete after exposure to elevated temperatures, Constr. Build. Mater. 35 (2012), https://doi.org/10.1016/j.conbuildmat.2012.05.031.

[89] J. Xie, Z. Zhang, Z. Lu, M. Sun, Coupling effects of silica fume and steel-fiber on the compressive behaviour of recycled aggregate concrete after exposure to elevated temperature, Constr. Build. Mater. 184 (2018), https://doi.org/10.1016/j.conbuildmat.2018.07.035.

[90] Y.C. Guo, J.H. Zhang, G.M. Chen, Z.H. Xie, Compressive behaviour of concrete structures incorporating recycled concrete aggregates, rubber crumb and reinforced with steel fibre, subjected to elevated temperatures, J. Clean. Prod. 72 (2014), https://doi.org/10.1016/j.jclepro.2014.02.036.

[91] J. Kim, G.P. Lee, D.Y. Moon, Evaluation of mechanical properties of steel-fibre-reinforced concrete exposed to high temperatures by double-punch test, Constr. Build. Mater. 79 (2015), https://doi.org/10.1016/j.conbuildmat.2015.01.042.

[92] W. Zheng, B. Luo, Y. Wang, Compressive and tensile properties of reactive powder concrete with steel fibres at elevated temperatures, Constr. Build. Mater. 41 (2013), https://doi.org/10.1016/j.conbuildmat.2012.12.066.

[93] M. Nematzadeh, A. Karimi, S. Fallah-Valukolaee, Compressive performance of steel fiber-reinforced rubberized concrete core detached from heated CFST, Constr. Build. Mater. 239 (2020), https://doi.org/10.1016/j.conbuildmat.2019.117832.

[94] P. Pliya, A.L. Beaucour, A. Noumowé, Contribution of cocktail of polypropylene and steel fibres in improving the behaviour of high strength concrete subjected to high temperature, Constr. Build. Mater. 25 (4) (2011), https://doi.org/10.1016/j.conbuildmat.2010.11.064.

[95] J. Yang, B. Chen, C. Nuti, Influence of steel fiber on compressive properties of ultra-high performance fiber-reinforced concrete, Constr. Build. Mater. 302 (2021), https://doi.org/10.1016/j.conbuildmat.2021.124104.

[96] X. Hou, M. Abid, W. Zheng, G.Q. Waqar, Evaluation of residual mechanical properties of steel fiber-reinforced reactive powder concrete after exposure to high temperature using nondestructive testing, Procedia Eng. (2017), https://doi.org/10.1016/j.proeng.2017.11.118.

[97] B. Chen, J. Liu, Residual strength of hybrid-fiber-reinforced high-strength concrete after exposure to high temperatures, Cem. Concr. Res. 34 (6) (2004), https://doi.org/10.1016/j.cemconres.2003.11.010.

[98] X. Zhang, X. Lin, Y. Chen, Study on mechanical properties of steel fiber reinforced nano-concrete (SFRNC) after elevated temperature, Compos. Struct. 268 (2021), https://doi.org/10.1016/j.compstruct.2021.113941.

[99] W. Zheng, B. Luo, Y. Wang, Stress–strain relationship of steel-fibre reinforced reactive powder concrete at elevated temperatures, Mater. Struct./Materiaux et Constructions 48 (7) (2015), https://doi.org/10.1617/s11527-014-0312-9.

[100] S. Khan, et al., Predicting the ultimate axial capacity of uniaxially loaded cfst columns using multiphysics artificial intelligence, Materials (Basel) 15 (1) (2022), https://doi.org/10.3390/ma15010039.

[101] J. Zhang, Y. Huang, G. Ma, B. Nener, Mixture optimization for environmental, economical and mechanical objectives in silica fume concrete: a novel frame-work based on machine learning and a new meta-heuristic algorithm, Resour. Conserv. Recycl. 167 (2021) 105395, https://doi.org/10.1016/j.resconrec.2021.105395. Apr.

[102] P. Dunlop S. Smith, Estimating key characteristics of the concrete delivery and placement process using linear regression analysis, Civ. Eng. Environ. Syst. 20 (4) (2003) 273–290.

[103] K. Sakino, H. Nakahara, S. Morino, I. Nishiyama, Behavior of centrally loaded concrete-filled steel-tube short columns, J. Struct. Eng. 130 (2) (2004) 180–188, https://doi.org/10.1061/(ASCE)0733-9445(2004)130:2(180). Feb.

[104] M.A. Haque, B. Chen, M.F. Javed, F.E. Jalal, Evaluating the mechanical strength prediction performances of fly ash-based MPC mortar with artificial intelligence approaches, J. Clean. Prod. 355 (2022) 131815, https://doi.org/10.1016/J.JCLEPRO.2022.131815. Jun.

[105] M.A. Shahin, Genetic programming for modelling of geotechnical engineering systems. Handbook of Genetic Programming Applications, Springer International Publishing, Cham, 2015, pp. 37–57, https://doi.org/10.1007/978-3-319-20883-1_2.

[106] A.A.H.M.M.R.N.F.M. Gandomi, Nonlinear genetic-based models for prediction of flow number of asphalt mixtures, J. Mater. Civ. Eng. 23 (2011) 248–263.

[107] A.H. Gandomi, D.A. Roke, Assessment of artificial neural network and genetic programming as predictive tools, Adv. Eng. Softw. 88 (2015) 63–72, https://doi.org/10.1016/j.advengsoft.2015.05.007. Oct.

[108] A. Golbraikh, A. Tropsha, Beware of q2!, J. Mol. Graph. Model. 20 (4) (2002) 269–276, https://doi.org/10.1016/S1093-3263(01)00123-1. Jan.

[109] P.P. Roy, K. Roy, On some aspects of variable selection for partial least squares regression models, QSAR. Comb. Sci. 27 (3) (2008), https://doi.org/10.1002/qsar.200710043.

[110] A. Ashrafian, F. Shokri, M.J. Taheri Amiri, Z.M. Yaseen, M. Rezaie-Balf, Compressive strength of Foamed Cellular Lightweight Concrete simulation: new development of hybrid artificial intelligence model, Constr. Build. Mater. 230 (2020), https://doi.org/10.1016/j.conbuildmat.2019.117048.

[111] S.M. Lundberg G.G. Erion S.I. Lee, "Consistent individualized feature attribution for tree ensembles.," 2018.

[112] M.M. Islam, et al., Prediction of compressive strength of high-performance concrete using optimization machine learning approaches with SHAP analysis, J. Build. Pathol. Rehab. 9 (2) (2024) 1–20, https://doi.org/10.1007/S41024-024-00445-Z/METRICS. Dec.

[113] A. Kashem, R. Karim, S.C. Malo, P. Das, S.D. Datta, M. Alharthai, Hybrid data-driven approaches to predicting the compressive strength of ultra-high-performance concrete using SHAP and PDP analyses, Case Stud. Constr. Mater. 20 (2024), https://doi.org/10.1016/j.cscm.2024.e02991.

[114] R. Kumar Tipu, V.R. Panchal, K.S. Pandya, An ensemble approach to improve BPNN model precision for predicting compressive strength of high-performance concrete, Structures 45 (2022) 500–508, https://doi.org/10.1016/J.ISTRUC.2022.09.046. Nov.

[115] A.A. Shahmansouri, H.Akbarzadeh Bengar, S. Ghanbari, Compressive strength prediction of eco-efficient GGBS-based geopolymer concrete using GEP method, J. Build. Eng. 31 (2020) 101326, https://doi.org/10.1016/j.jobe.2020.101326. Sep.

[116] M.I. Shah, S.A. Memon, M.S. Khan Niazi, M.N. Amin, F. Aslam, M.F. Javed, Machine learning-based modeling with optimization algorithm for predicting mechanical properties of sustainable concrete, Adv. Civil Eng. 2021 (1) (2021) 6682283, https://doi.org/10.1155/2021/6682283. Jan.

[117] M.I. Shah, et al., Performance evaluation of soft computing for modeling the strength properties of waste substitute green concrete, Sustainability. 13 (2021) 2867, https://doi.org/10.3390/SU13052867. *Page*vol. 13, no. 5, p. 2867, Mar. 2021.

[118] K.E. Taylor, Summarizing multiple aspects of model performance in a single diagram, J. Geophys. Res. Atmos. 106 (D7) (2001), https://doi.org/10.1029/2000JD900719.

[119] H.H. Awan, et al., Predicting Marshall flow and marshall stability of asphalt pavements using multi expression programming, Buildings 12 (2022) 314, https://doi.org/10.3390/BUILDINGS12030314. *Page*vol. 12, no. 3, p. 314, Mar. 2022.
[120] D.C. Montgomery, E.A. Peck, G.G. Vining, Introduction to Linear Regression Analysis, John Wiley & Sons., 2021.
[121] Y. Li, et al., The effects of rock index tests on prediction of tensile strength of granitic samples: a neuro-fuzzy intelligent system, Sustainability. 13 (19) (Sep. 2021) 10541, https://doi.org/10.3390/su131910541.
[122] X. Ren, Y. Ding, Q. Liu, S. Chen, F. Song, Effect of different volume fraction of steel fiber/graphite on thermal conductivity and compressive properties of concrete, Front. Mater. 9 (2022), https://doi.org/10.3389/fmats.2022.1003830.
[123] M. Nematzadeh, A.A. Shahmansouri, R. Zabihi, Innovative models for predicting post-fire bond behavior of steel rebar embedded in steel fiber reinforced rubberized concrete using soft computing methods, Structures 31 (2021), https://doi.org/10.1016/j.istruc.2021.02.015.